Fabrication and VMD performance of TiO_2 nanocomposite PVDF membranes and PVDF-PTFE composite membranes

Zhelun Li

A thesis submitted to the

Faculty of Graduate and Postdoctoral Studies in partial fulfillment of the

requirements for the

Master of Applied Science in Chemical Engineering

University of Ottawa

Abstract

In this study, two different strategies were carried out to modify the polyvinylidene fluoride (PVDF) distillation membrane for desalination. The first strategy was the addition of TiO_2 nanoparticles into the target membranes and a synergistic effect of hydrophilic and hydrophobic nanoparticles was found for the first time in this work. And the other strategy was the introduction of another polymer material, polytetrafluoroethylene (PTFE), to the PVDF membranes to fabricate a flat sheet PVDF-PTFE composite membrane and this is the first attempt that such a membrane to be made. Two types of membranes were characterized by scanning electron microscopy (SEM) detection, porosity measurement, energy dispersive X-ray spectroscopy (EDX), Attenuated total reflectance (ATR)-Fourier transformed infrared spectroscopy (FTIR), contact angle (CA) measurement, atomic force spectroscopy (AFM) detection and liquid entry pressure of water (LEPw) measurement. Their performance was evaluated by vacuum membrane distillation (VMD) experiments. And the best VMD pure water permeate flux of the membranes fabricated under these two modify strategies could achieve 4.26 kg/m^{2}h (M-L5-B2) and 5.61 kg/m^{2}h (M-40), respectively, when that of pure PVDF membrane is only 0.71 kg/m^{2}h. The salt rejection of the prepared composite membranes are all stably higher than 99.5% which demonstrate their capacity for desalination.

Keywords: membrane distillation, membrane modification, composite membrane

Résumé

Dans cette étude, deux stratégies différentes ont été mises en œuvre pour modifier la membrane de distillation du fluorure de polyvinylidène (PVDF) pour le dessalement. La première stratégie était l'ajout de nanoparticules de TiO_2 dans les membranes cibles et un effet synergique des nanoparticules hydrophiles et hydrophobes a été trouvé pour la première fois dans ce travail. Et l'autre stratégie était l'introduction d'un autre matériau polymère, le polytétrafluoroéthylène (PTFE), sur les membranes de PVDF pour fabriquer une membrane composite en feuille de PVDF-PTFE plat et c'est la première tentative qu'une telle membrane soit faite. Deux types de membranes ont été caractérisés par la détection par microscopie électronique à balayage (MEB), la mesure de porosité, la spectroscopie à rayons X dispersive (EDX), la réflectance totale atténuée (ATR), la spectroscopie infrarouge transformée de Fourier, la mesure de l'angle de contact, la détection par spectroscopie de force atomique (AFM) et la mesure de la pression d'entrée des liquides (LEPw). Leur performance a été évaluée par des expériences de distillation à membrane sous vide (VMD). De plus, le meilleur flux de perméat d'eau pure VMD des membranes fabriquées sous ces deux stratégies de modification pourrait atteindre respectivement 4.26 kg/m^2h (M-L5-B2) et 5.61 kg/m^2h (M-40), alors que celui de la membrane PVDF pure soit seulement 0.71 kg/m^2h. Les rejets de sel des membranes composites préparées sont tous supérieurs à 99.5% sous une forme stable, ce qui démontre leur capacité de dessalement.

mots clés: membrane distillation, membrane de modification, membrane composite

Acknowledgment

I would like to express my sincerest and heartfelt appreciation to my supervisor and co-supervisor, Dr. Christopher Q. Lan and Dr. Takeshi Matsuura, for their valued and patient guidance, background knowledge and support. My gratitude also goes to Dr. Dipak Rana for his patient guidance, precious help and background knowledge in the completion of this study.

My deepest gratitude is also extended to all staff in the Department of Chemical and Biological Engineering in the Faculty of Engineering, University of Ottawa, especially Sylvie Saindon, Francine Pétrin and Franco Ziroldo for their valuable help in official and technical affair.

I acknowledge the Nanjing Tech. University and Dr. Zhaohui Wang, for their help in SEM and AFM test in my first project, as well as Carleton SEM lab and Dr. Jianqun Wang, for their help with SEM and EDX test in my second project.

Arkema Inc. (Philadelphia, PA, USA) is also appropriated for the gift of polyvinylidene fluoride powder and particles.

Gratitude is also extended to Viyash Murugesan， Johnson E. Efome, Mohammad Ali Baghbanzadeh for their inspiration, support and guidance in my study and research.

Finally, I am grateful to my beloved parents for their generous love, support and encouragement in my life.

Table of Contents

List of Figures

List of Tables

Legend

C_p	heat capacity of feed water (J/kg K)
G_r	Grashof number
h_f	heat transfer coefficient (W/m^2K)
J_m	permeate flux through the membrane (kg/ m^2h)
K_m	mass transfer coefficient (kg/m^2 s Pa)
N_u	Nusselt number
p_{mf}, p_{mp}	the particle water vapor pressure at the membrane surface on the feed side and the permeate side (-)
P_r	Prandtl number
Q_{total}, Q_f, Q_m	the heat flux through the whole process, from feed bulk to the feed side membrane surface, and through the membrane (W/m^2)
R	universal gas constant (8.314×10^{-3}J/kmol K)
r	membrane pore radius (m)
T_{mf}, T_{bf}	temperature at membrane surface of feed side and feed bulk

Greeks

λ	mean free path of the vapor molecule (-)
ε	membrane porosity (-)
τ	pore tortuosity (-)
δ	membrane thickness (m)
μ	viscosity of feed water (Pa s)
β	volume thermal expansion of feed water ($1/K$)

Chapter 1. Introduction

Fresh water shortage has been recognized as one of the major current challenges and in the coming future, because of the fast depletion of ground water. It has been estimated that around 1.8 billion people world wide would suffer absolute water scarcity and two third of the population around the world would be impact by the water shortage in 2025. However, another fact is, nearly 97% of all the earth's water is seawater which has not been utilized sufficiently, and as a result, desalination technology, considered as an effective way to solve fresh water crisis, is attracting more and more attentions over the past few decades. [1–5]

And the commonly used desalination technologies could be divided into two major categories, thermal processes and membrane-based processes. Thermal processes include Multiple Effect Distillation (MED), Mechanical Vapor Compression (VC) while membrane based processes include Reverse Osmosis (RO), Forward Osmosis (FO), Ultrafiltration (UF), Microfiltration (MF), Nanofiltration (NF), and Membrane Distillation (MD), among which the membrane based processes dominates the desalination technologies market as it attributes to more than 60% of the desalination water. [6–8]

Among the mentioned membrane-based processes, MD is a relatively new technology for desalination. And this technology is attracting more and more attentions because of its low energy consumption and mild operating conditions. A large number of studies

have been carried out to further develop this technology during the past decades. However, several drawbacks still exist in MD processes, such as the low efficiency caused by the low permeate flux, the significant temperature and concentration polarizations, the low durability when dealing with high temperature feeds and/or high operating pressures. Thus, various modification methods were proposed to enhance the MD membranes and modules.

In this thesis, two different types of MD membrane fabrication strategies were investigated. The first method was presented in Chapter 3, in which the membrane was modified by adding inorganic nanoparticles to fabricate nanocomposite membranes. Both hydrophilic and hydrophobic nanoparticles were investigated in this research and they both exhibit great potential in enhancing membrane performance in term of permeability and LEPw. Chapter 4 presents another modification strategy, in which two different polymers were used together to fabricate a flat sheet PVDF-PTFE composite membrane was fabricated by phase inversion method,

Reference

[1] N. Ghaffour, T.M. Missimer, G.L. Amy, Technical review and evaluation of the economics of water desalination: Current and future challenges for better water supply sustainability, Desalination. 309 (2013) 197–207. doi:10.1016/j.desal.2012.10.015.

[2] J. Yin, B. Deng, Polymer-matrix nanocomposite membranes for water treatment, J. Memb. Sci. 479 (2015) 256–275. doi:10.1016/j.memsci.2014.11.019.

[3] A.S. Hassan, H.E.S. Fath, Review and assessment of the newly developed MD for desalination processes, Desalin. Water Treat. 51 (2013) 574–585. doi:10.1080/19443994.2012.697273.

[4] R.K. McGovern, J.H. Lienhard V, On the potential of forward osmosis to energetically outperform reverse osmosis desalination, J. Memb. Sci. 469 (2014) 245–250. doi:10.1016/j.memsci.2014.05.061.
[5] L. Karimi, L. Abkar, M. Aghajani, A. Ghassemi, Technical feasibility comparison of off-grid PV-EDR and PV-RO desalination systems via their energy consumption, Sep. Purif. Technol. 151 (2015) 82–94. doi:10.1016/j.seppur.2015.07.023.
[6] W.G. Shim, K. He, S. Gray, I.S. Moon, Solar energy assisted direct contact membrane distillation (DCMD) process for seawater desalination, Sep. Purif. Technol. 143 (2015) 94–104. doi:10.1016/j.seppur.2015.01.028.
[7] J.G. Lee, Y.D. Kim, W.S. Kim, L. Francis, G. Amy, N. Ghaffour, Performance modeling of direct contact membrane distillation (DCMD) seawater desalination process using a commercial composite membrane, J. Memb. Sci. 478 (2015) 85–95. doi:10.1016/j.memsci.2014.12.053.
[8] M.A.E.R. Abu-Zeid, Y. Zhang, H. Dong, L. Zhang, H.L. Chen, L. Hou, A comprehensive review of vacuum membrane distillation technique, Desalination. 356 (2015) 1–14. doi:10.1016/j.desal.2014.10.033.

Chapter 2. Literature Review

2.1 Introduction

During the last decades, membrane separation technology has made a great progress and membrane processes have been approved to be competitive to the conventional separation methods, such as multiple effect distillation (MED), multi-stage flash distillation (MSF), mechanical vapor compression (MVC), in a wide variety of applications. Different membrane separation processes have been developed during the past half century and several new membrane applications are constantly emerging from laboratories and industries. [1–3]

Membrane distillation (MD) technology is one of the emerging membrane-based separation process which was driven by the vapor pressure difference caused by the different temperatures at the feed side and the permeate side. The great potential of this process has been demonstrated by several studies in many types of applications, such as desalination. wastewater treatment and the separation of volatile components from liquid mixtures. [4–10] The characteristic of the MD process should contain the following characteristics [11]:

1. The membrane should be porous.
2. The membrane used should be hydrophobic and not wetted by the process liquids.
3. The process does not alter the VLE of the involved.

4. Only vapor was allowed to transport pass though the membrane does not permit vapor condensation to occur inside its pores.
5. The membrane is maintained in direct contact at least with the hot feed liquid solution to be treated in the process.

In term of desalination application, membrane separation technology plays a dominated role as it contributes to more than 60% of the water produced by desalination. Traditional membrane separation processes that are applicable to desalination include reverse osmosis (RO), forward osmosis (FO), in which RO is currently the leading technology because of its low energy consumption, high permeability and technology maturity on a comparative basis[12,13]. However, as an emerging membrane separation technology, MD was considered to have the capacity to rival RO processes in the near future. Table 2-1 compares the MD and RO in term of several aspects of the desalination process.

Table 2-1

Comparison between MD and RO for desalination

Process	RO	MD
Fouling potential	High	Low
Ability to handle the high concentration feed	Unable	Able
Feed pre-treatment	Necessary	Unnecessary
Electrical energy consumption	High	Low

Thermal energy consumption	Low	High
Operating conditions	Harsh	Mild

2.2 Different Kinds of Membrane Distillation Configuration

Several types of configurations were employed in treating feed solutions in MD process, which are differ with each other according to the different structure of the permeate side. Some of the major MD configurations include [14,15]:

2.2.1 Direct Contact Membrane Distillation (DCMD)

DCMD is the simplest MD configuration. As shown in Fig. 2-1, this kind of configuration requires the feed solution with a relatively higher temperature in direct contact with the top surface of the membrane, while the water with a lower temperature at permeate side flow through the other membrane surface. Because of its simple structure and high flux, DCMD was exposed to a large amount of laboratory researches. The main disadvantage of this configuration is its low energy efficiency which limits its commercialization. Because of the higher heat transfer coefficient on the permeate side, DCMD has the highest heat conduction loss among all MD configurations which will decrease its thermal efficiency in the real applications[5,16–18].

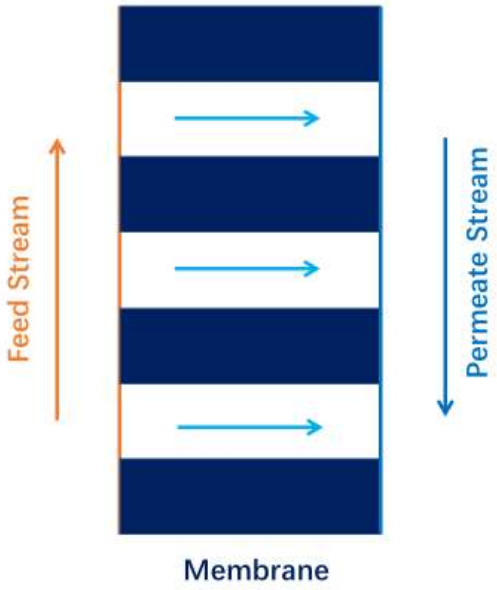

Fig.2-1 The schematic of DCMD

2.2.2 Air Gap Membrane Distillation (AGMD)

The schematic of AGMD is shown in Fig. 2-2. The high temperature feed solution is in direct contact with top surface of the membrane. Air is then trapped between the membrane and the condensation surface. The vapor travels through the air gap and condense at the cold surface of membrane module. And this configuration has a relatively lower heat losses caused by conduction when compared with DCMD process.[14]

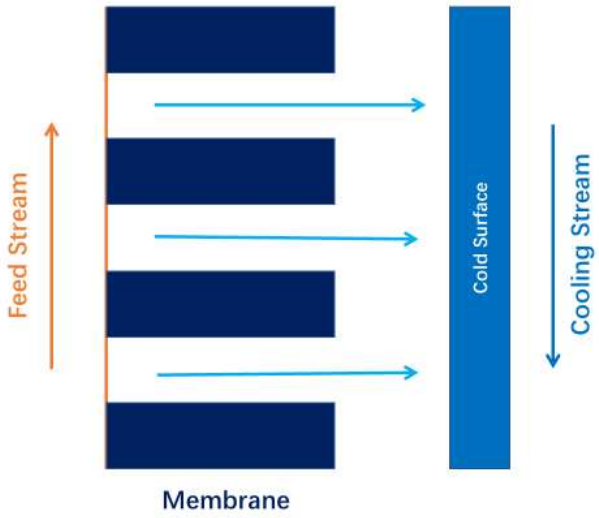

Fig.2-2 The schematic of AGMD

2.2.3 Sweeping Gas Membrane Distillation (SGMD)

The SGMD schematic is presented in Fig. 2-3. In SGMD process, there is an inert gas sweeping through the permeate side of the membrane module and carry the vapor that leave the membrane. Vapor was condensed and collected in an external condenser. SGMD is widely used to remove volatiles from an aqueous solution. And because of the greater driving force, SGMD has a relatively higher mass transfer efficient and lower heat loss across the membrane in comparation with AGMD and DCMD, respectively. However, the employing of the external condenser and inert gas blower would highly increase its operating costs.[14]

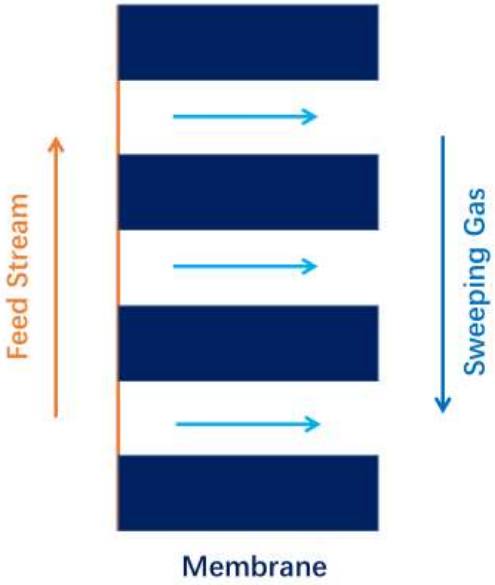

Fig.2-3 The schematic of SGMD

2.2.4 Vacuum Membrane Distillation （VMD）

The schematic of VMD configuration is shown in Fig. 2-4. In VMD configuration, a vacuum pump was employed at the permeate side to produce a vacuum environment and induce the transport of the vapor through the membrane pores. The condensation of the vapor occurs at the outside of the module with negligible heat loss because of the conduction.[17,19–21]

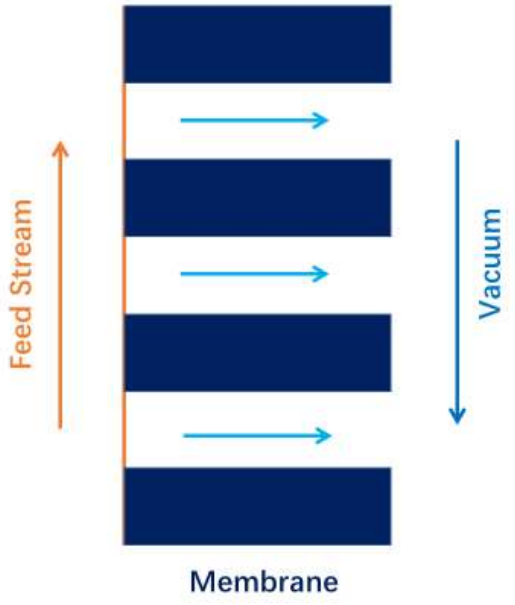

Fig.2-4 The schematic of VMD

2.3 Distillation Membrane Materials and Fabrication

The most commonly-used materials for membrane distillation include PVDF, PTFE, and PP. Among which the PTFE has the highest hydrophobicity, plus good thermal and chemical stability, this makes it a ideal material for membrane distillation.[11,14,17] However, its high thermal conductivity also results in higher heat losses and the fabrication of PTFE is a harsh process requiring high temperature, these limit the application of this material. Meanwhile, PVDF and PP membranes also show appropriate hydrophobicity, thermal and chemical resistance and mechanical strength. Thus, PVDF and PP are also popular materials for MD. [22–24] MD membranes are fabricated by different techniques, that include sintering, stretching method, and phase inversion.[3,24]

The sintering method could be applied to fabricate PTFE membranes. In this method, polymeric powder is pressed into a film or plate, and then sintered below the melting point to obtain the final membranes. The stretching method was usually applied to fabricate PP and PTFE membranes. Polymeric layers are formed by extrusion from a polymeric powder at temperatures near the melting point that is combined with a rapid draw-down.

PVDF is the most easy-handling membrane fabrication material among these three materials, which could be made by phase inversion method. [17,25]In this method, a polymeric solution is prepared using an appropriate solvent and cast as a thin layer before the cast membrane is immersed in a non-solvent medium to induce the phase inversion and form the membranes. Phase inversion method is considered as the mildest fabrication method among these methods as it does not require a high temperature.

2.4 Membrane Modification Methods for MD

Generally, there are several surface and bulk membrane modification methods applied to improve the performance of the MD membranes as following:

2.4.1 Adding Nanoparticles

Our research group has demonstrated that adding nanoparticles to the dope solution to fabricate nanocomposite membrane has been demonstrated to be an effective way to enhance the MD membrane properties and the membrane performance [7,9,10].

In this modification method, desired amount and type of nanoparticles were blended into the membrane dope solution directly and dispersed well in the solution via ultra-sound sonication treatment or over-head stirring. The blended dope solution was then applied for membrane fabrication and the nanocomposite membrane could be thus formed.

According to our previous researches, both hydrophobic and hydrophilic nanoparticles present great potential for membrane properties and performance enhancement. Both particles could enhance the permeate flux performance of the target membrane while maintaining a nearly absolute salt rejection in desalination at the same time. The top surface and cross-sectional morphology were also changed in nanocomposite membranes in comparison with the pure membranes.

2.4.2 Other Modification Methods

2.4.2.1 Radiation Graft Polymerization

Radiation graft polymerization was commonly used for fabrication of separation membranes with good ability and performance for applications such as dialysis, reverse osmosis and electrolysis processes. The grafting types include chemical grafting, plasma grafting, thermal grafting and photo grafting [15].

2.4.2.2 Plasma Polymerization

Plasma polymerization refers to a membrane modification method in which active particles generated by splitting and decomposing organic monomers under glow discharge were recombined to form polymers on the top surface of a membrane substrate. Several researches have been carried out to prepare selective membranes with high performance for different applications using plasma polymerization. In this modification process, many types of volatile organic molecules with or without chemical functional groups could be reacted and then generate a polymer [15].

2.4.2.3 Surface Coating

Surface coating, which is also known as dip coating or solution coating. In this modification, a coating layer over the target porous membrane was generated by depositing a polymer solution onto the top surface directly. The coating layer material could be hydrophobic to enhance the surface hydrophobicity of the membrane or hydrophilic to prevent the pore wetting of the support layer. [14]

2.4.2.4 Surface Modification by SMMs

It has been confirmed by several researches that the polymer which has a lower surface energy would migrate to air/membrane interface during the membrane forming process to reduce the interfacial tension when different polymers were mixed. Based on this, surface modifying macromolecule (SMM) surface modification method which is known as one of the simplest modification method for MD membranes was thus

proposed. In this method, synergized SMM was added to the membrane dope solution and then the hydrophobic SMM with a low surface energy will migrate and concentrate at the membrane top surface (air/membrane interface) during the membrane forming process and thus, modify the membrane surface property. It has been claimed that the adding of SMM will enhance the membrane mechanical strength as well as the membrane surface hydrophobicity. [14]

2.5 Membrane Characteristics in MD

The membrane that are applied to MD process should have low resistance to mass transfer to obtain a substantial permeate flux, good thermal stability and low thermal conductivity to prevent trans-membrane heat losses and resistance to chemicals. [1,3,4,11,14,26–29]. Usually, the membrane for MD process should be characterized as follows:

2.5.1 Liquid entry pressure (LEP)

Liquid entry pressure (LEP), which also known as wetting pressure, is the pressure difference at which the liquid penetrates into the largest pores of the hydrophobic membrane. This critical pressure difference was mainly determined by the interfacial tension, the contact angle of the liquid on the surface (surface hydrophobicity), temperature as well as the size and shape of membrane pores (especially the maximum pore size). A high LEP value is preferred in MD process, as higher LEP demonstrates a stronger resistance to the liquid entering the membrane pores and the objective is that

the membrane pores are only filled with vapor. And by measuring LEP, one can get the pressure limit in the MD process.

Eq.2-1 below (Young-Laplace equation) could be utilized to determine the LEP value of a MD membrane:

$$\Delta P = P_f - P_p = \frac{-2B\gamma_1 \cos\theta}{r_{max}} \quad (2\text{-}1)$$

Where P_f and P_p represent the hydraulic pressure at the feed and permeate side, respectively; B is a geometric pore coefficient (equal to 1 for cylindrical pore); γ_1 represents the liquid surface tension; θ and r_{max} are contact angle of the liquid on membrane top surface and maximum pore size, respectively. As can be clearly detected from the equation, the larger the maximum pore size is, the lower the LEP will be and the membrane will be less suitable for the MD process due to the likely pore wetting. Thus, reducing the largest pore size while maintaining the surface porosity is desired for MD membranes.

2.5.2 Membrane Thickness

Membrane thickness was considered as a large impact on the membrane permeate flux in MD process, and a thicker membrane usually results a lower permeate flux.[6] It could be explained by the increasing mass transfer resistance when the membrane becomes thicker. However, a thick membrane also indicates a lower heat loss in MD

process, which means a thicker membrane does not always demonstrate a better membrane.[30] According to Lagana et al[14], the optimum membrane thickness for MD process is in the range from 30 to 60 μm, considering both of the mass transfer and heat loss.

2.5.3 Membrane Porosity and Pore Tortuosity

Membrane porosity refers to the ratio of the volume of the membrane pores and macro-voids to the total membrane volume. It could vary from 35% to 85% in different types of membranes. [13,31] In most cases, higher porosity indicates a higher thermal resistance and lower conductive heat loss as air in the membrane macro-voids has a relatively lower thermal conductivity in comparation with the membrane matrix. Moreover, higher membrane porosity could also increase the permeability of MD membrane because of the larger evaporation surface area. Thus, in term of permeate flux and heat efficiency, a high membrane porosity is preferred for MD processes. However, the increment of membrane porosity could also decrease the mechanical strength of the membrane, which would result in a membrane with a high tendency to crack and cause water leakage during the membrane operation. Eq. 2-2 (Smolder-Franken Equation) below could be used for determination of the porosity:

$$\varepsilon = 1 - \frac{\rho_m}{\rho_{pol}} \tag{2-2}$$

Where ρ_m and ρ_{pol} represent the densities of membrane and polymer material,

respectively.

Tortuosity is a parameter which was used to determine the deviation of the pore structure from a cylindrical shape. Higher tortuosity indicates a more complicated transportation path and accordingly a smaller permeate flux. By using τ and ε represent tortuosity and porosity, respectively, it was suggested that following equation could be used to determine the relationship between porosity and tortuosity[14,32]

$$\tau = \frac{(2-\varepsilon)^2}{\varepsilon} \quad (2\text{-}3)$$

2.5.4 Mean Pore Size and Pore Size Distribution

Based on several previous studies, MD membranes usually have a pore size in the range from 0.1 to 1 μm, and permeate flux always increases with the increment of membrane pore size. The mean pore size is usually used to characterize the membrane due to the ununiform distribution of membrane pore sizes. Though a large average pore size always indicates a high permeate flux, the membrane pore size should also be small enough to avoid the occurrence of pore wetting during the MD process. Thus, an optimum pore size is required depending upon the operating conditions and the feed being treated. Khayet et al [33] suggested that, mean pore size plays a more important role in determining the membrane vapor flux, instead of pore size distribution. Scanning Electron Microscopy (SEM) and Atomic Force Microscopy (AFM) could be employed to determine surface morphology of an MD membrane, and the porosity, pore size, and

pore size distribution of a membrane could thus be measured and analyzed.

2.5.5 Scanning Electron Microscopy (SEM)

The membrane top surface and cross-sectional morphology are usually characterized by SEM imaging, and the SEM images could also be further used to estimate the porosity, pore size, pore size distribution and membrane thickness by employing image-analyzing software. [1,34,35] SEM images are formed when a beam of high energy electrons hits the atoms on the surface of the sample (usually coated with gold), resulting in the release of low energy atoms from the sample which are then detected to produce a micrographic image.

2.5.6 Atomic Force Microscopy (AFM)

In MD membrane characterization process, AFM tests are usually carried out to detect the membrane surface morphology. A 3-D image could be obtained during the AFM detection, in which we can observe the surface 3-D morphology. Built-in computer software bundle with the AFM equipment could also help calculate the roughness parameters of the membranes.[7,8,10,25]

2.6 Transport Phenomena in MD

2.6.1 Mass Transfer

The transport process in VMD is divided into the following three steps: (1) transport from the feed bulk to the membrane surface (feed side); (2) transport through the membrane pores from the feed to the permeate side; (3) transport from the membrane surface (permeate side) to the condenser surface [36–39]. In the VMD process, in which this thesis focuses on, the first and the third steps could be ignored, for the reasons that diffusion inside the pores of the vapor molecules at the feed/membrane interface is favored, and also that the mass transfer resistance is neglected on the permeate side due to vacuuming. The membrane mass transfer coefficient (K_m) can be calculated based on the Fick's law[40]:

$$J = J_m = K_m(p_m - p_v) \tag{2-4}$$

Where J is the VMD flux (kg/m^2 s); J_m is the flux through the membrane (kg/m^2 s), p_v is the pressure (Pa) at the permeate side membrane surface which is close to vacuum in the VMD process, p_m is the water vapor pressure (Pa) at the feed side membrane surface. The latter is calculated by the Antoine equation[41]:

$$p_m(T_m) = \exp(23.1964 - \frac{3816.44}{T_m - 46.13}) \tag{2-5}$$

The membrane mass transfer coefficient K_m is determined by three mechanisms, the Knudsen diffusion, viscous flow and molecular diffusion. Among these the molecular diffusion can be neglected in this process due to the small amount of air exist in the

membrane pores.

The mean free path of water molecules are given as[14,32]:

$$\lambda = \frac{k_B T}{\sqrt{2}\pi p_{average} d_p^2} \tag{2-6}$$

where k_B is the Boltzmann constant (J/K), T is the absolute temperature (K) which can be replaced by T_{mf}, while $p_{average}$ is the average pressure inside the membrane pore which was given by $(p_{mp} + p_{mf})/2$.

When the membrane pore diameter d (m) is smaller than 0.1λ, the molecule -pore wall collisions dominants the mass transfer through the membrane, which was defined as Knudsen diffusion. On the other hand, when d is larger than 100λ, the mass transfer through the membrane was dominated by the molecular-molecular collision, which was also called viscous flow. For d between 0.1λ and 100λ, both Knudsen diffusion and viscous flow attribute effect to mass transfer. In this work, the mean free path, λ, is in the range of $6.5 - 8.5 \times 10^{-7} m$, while the membrane pore diameter, d, is in the range of 0.11-0.16 μm, which means both the Knudsen diffusion and viscous flow should be considered. And the K_m can also be represented as:

$$K_m = K_{knudsen} + K_{viscous} \tag{2-7}$$

where the $K_{knudsen}$ and $K_{viscous}$ are given as

$$K_{knudsen} = \frac{2}{3}\frac{r\varepsilon}{\tau\delta}\sqrt{\frac{8M}{\pi RT}} \quad (2\text{-}8)$$

$$K_{viscous} = \frac{r^2\varepsilon Mp}{8\tau\delta\mu RT} \quad (2\text{-}9)$$

where $r\,(m)$, $\varepsilon(-)$, $\tau(-)$, $\delta(\mathrm{m})$, $\mu(Pa\ s)$ are membrane pore radius, membrane porosity, pore tortuosity, membrane thick and the water vapor viscosity, respectively. M ($18.02\ kg/kmol$) is the water molecular weight and R ($8.314 \times 10^3\ J/kmol$ K) is the molar gas constant. Combining the two above equations:

$$K_m = K_{knudsen} + K_{viscous} = \frac{2}{3}\frac{r\varepsilon}{\tau\delta}\sqrt{\frac{8M}{\pi RT}} + \frac{r^2\varepsilon Mp}{8\tau\delta\mu RT} \quad (2\text{-}10)$$

2.6.2 Heat Transfer

The heat transfer process of VMD consists of three paths, which are the feed bulk to the feed side membrane surface, feed side membrane surface to that of permeate side, from permeate side membrane surface to the condenser surface. However, the heat conduction from permeate side membrane surface to the condenser surface is too low to be considered due to low pressure which is close to vacuum. [42]

For the heat transfer from feed bulk to the membrane surface at feed side, the heat flux is given by:

$$Q_f = h_f(T_{bf} - T_{mf}) \quad (2\text{-}11)$$

where $Q_f(W/m^2)$ is the heat flux from feed bulk to the membrane surface at feed side through the liquid boundary layer; T_{bf} and T_{mf} are temperatures of feed bulk and feed side membrane surface, respectively; and $h_f(W/m^2\,K)$ is the heat transfer coefficient. These coefficients can be calculated using Nusselt number (N_u):

$$h_f = \frac{N_u k}{L_c} \tag{2-12}$$

where L_c (m) and k (W/mK) are the characteristic length and the fluid thermal conductivity, respectively. N_u can be obtained by:

$$N_u = 0.53(P_r \cdot G_r)^{0.25} \text{ when } 10^3 < P_r \cdot G_r < 10^6 \tag{2-13-a}$$

$$N_u = 0.13(P_r \cdot G_r)^{0.33} \text{ when } 10^6 < P_r \cdot G_r < 10^{12} \tag{2-13-b}$$

where Prandtl number, P_r, and Grashof number, G_r, are given as[43]:

$$P_r = \frac{\mu C_p}{k} \tag{2-14-a}$$

$$G_r = \frac{L_c^3 \rho^2 \beta g (T_{bf} - T_{mf})}{\mu^2} \tag{2-14-b}$$

where μ (Pa s), C_p (J/kgK), ρ (kg/m^3), β $(1/K)$ are viscosity, heat capacity, density, volume thermal expansion of the feed water at given temperature, respectively, and g is the gravitational acceleration (9.8 m/s^2).

For the heat transfer process through the membrane (from the feed side membrane surface to the permeate side membrane surface), the heat flux is given as:

$$Q_m = J_m \Delta H_{evap} \quad (2\text{-}15)$$

where Q_m (W/m^2) and J_m (kg/m^2 s) are the heat and mass flux through the membrane, respectively, and ΔH_{evap} (kJ/kg) is the enthalpy of evaporation of water at the given temperature.

2.7 Concentration and Temperature Polarization

When dealing with high concentration solutions, the mass transfer in MD process will induce a concentration difference between the feed bulk and membrane surface and thus, form a different concentration boundary layer at feed/membrane interface. And this phenomenon is named concentration polarization. [14,44–49] As well, because of heat transfer in MD process, the temperature at the area close to membrane top surface will be lower than that of hot feed bulk solution and the temperature at membrane permeate surface will be higher than that of permeate bulk solution, and in consequence, a heat transfer boundary layer will also be formed and this was called temperature polarization. Both temperature and concentration polarization decrease the permeate flux of the membrane in MD process, and they are considered as a significant barrier in the development of MD technology.

Several researchers indicate that the temperature polarization has a larger impact of membrane performance than concentration polarization when feed concentration is lower that 5% as the heat transfer boundary layer around the membrane/feed and membrane/permeate interface is wider and larger than the different concentration boundary layer formed by concentration polarization.[5,33,50]

Reference

[1] N. Ghaffour, T.M. Missimer, G.L. Amy, Technical review and evaluation of the economics of water desalination: Current and future challenges for better water supply sustainability, Desalination. 309 (2013) 197–207. doi:10.1016/j.desal.2012.10.015.

[2] J. Yin, B. Deng, Polymer-matrix nanocomposite membranes for water treatment, J. Memb. Sci. 479 (2015) 256–275. doi:10.1016/j.memsci.2014.11.019.

[3] A.S. Hassan, H.E.S. Fath, Review and assessment of the newly developed MD for desalination processes, Desalin. Water Treat. 51 (2013) 574–585. doi:10.1080/19443994.2012.697273.

[4] M.A.E.R. Abu-Zeid, Y. Zhang, H. Dong, L. Zhang, H.L. Chen, L. Hou, A comprehensive review of vacuum membrane distillation technique, Desalination. 356 (2015) 1–14. doi:10.1016/j.desal.2014.10.033.

[5] J.G. Lee, Y.D. Kim, W.S. Kim, L. Francis, G. Amy, N. Ghaffour, Performance modeling of direct contact membrane distillation (DCMD) seawater

desalination process using a commercial composite membrane, J. Memb. Sci. 478 (2015) 85–95. doi:10.1016/j.memsci.2014.12.053.

[6] G. Guan, X. Yang, R. Wang, A.G. Fane, Evaluation of heat utilization in membrane distillation desalination system integrated with heat recovery, Desalination. 366 (2015) 80–93. doi:10.1016/j.desal.2015.01.013.

[7] Z. Li, D. Rana, Z. Wang, T. Matsuura, C.Q. Lan, Synergic effects of hydrophilic and hydrophobic nanoparticles on performance of nanocomposite distillation membranes: An experimental and numerical study, Sep. Purif. Technol. 202 (2018) 45–58. doi:10.1016/j.seppur.2018.03.032.

[8] Z. Chen, D. Rana, T. Matsuura, D. Meng, C.Q. Lan, Study on structure and vacuum membrane distillation performance of pvdf membranes: II. influence of molecular weight, Chem. Eng. J. 276 (2015) 174–184. doi:10.1016/j.cej.2015.04.030.

[9] M. Baghbanzadeh, D. Rana, C.Q. Lan, T. Matsuura, Effects of Inorganic Nano-Additives on Properties and Performance of Polymeric Membranes in Water Treatment, Sep. Purif. Rev. 45 (2016) 141–167. doi:10.1080/15422119.2015.1068806.

[10] J.E. Efome, M. Baghbanzadeh, D. Rana, T. Matsuura, C.Q. Lan, Effects of superhydrophobic SiO<inf>2</inf> nanoparticles on the performance of PVDF flat sheet membranes for vacuum membrane distillation, Desalination. 373 (2015) 47–57. doi:10.1016/j.desal.2015.07.002.

[11] E. Drioli, A. Ali, F. Macedonio, Membrane distillation: Recent developments

and perspectives, (2014). doi:10.1016/j.desal.2014.10.028.

[12] L. Karimi, L. Abkar, M. Aghajani, A. Ghassemi, Technical feasibility comparison of off-grid PV-EDR and PV-RO desalination systems via their energy consumption, Sep. Purif. Technol. 151 (2015) 82–94. doi:10.1016/j.seppur.2015.07.023.

[13] T.H. Chong, S.L. Loo, A.G. Fane, W.B. Krantz, Energy-efficient reverse osmosis desalination: Effect of retentate recycle and pump and energy recovery device efficiencies, Desalination. 366 (2015) 15–31. doi:10.1016/j.desal.2015.01.017.

[14] M.S. Khayet, T. Matsuura, Membrane distillation : principles and applications, Elsevier, 2011.

[15] T. Matsuura, M.S. Khayet, Membrane Distillation., An Elsevier Title, 2011.

[16] J. Wang, L. Zheng, Z. Wu, Y. Zhang, X. Zhang, Fabrication of hydrophobic flat sheet and hollow fiber membranes from PVDF and PVDF-CTFE for membrane distillation, J. Memb. Sci. 497 (2016) 183–193. doi:10.1016/j.memsci.2015.09.024.

[17] H. Fan, Y. Peng, Application of PVDF membranes in desalination and comparison of the VMD and DCMD processes, Chem. Eng. Sci. 79 (2012) 94–102. doi:10.1016/j.ces.2012.05.052.

[18] B.B. Ashoor, S. Mansour, A. Giwa, V. Dufour, S.W. Hasan, Principles and applications of direct contact membrane distillation (DCMD): A comprehensive review, Desalination. 398 (2016) 222–246.

doi:10.1016/j.desal.2016.07.043.

[19] A. Figoli, S. Simone, A. Criscuoli, S.A. Al-Jlil, F.S. Al Shabouna, H.S. Al-Romaih, E. Di Nicolò, O.A. Al-Harbi, E. Drioli, Hollow fibers for seawater desalination from blends of PVDF with different molecular weights: Morphology, properties and VMD performance, Polym. (United Kingdom). 55 (2014) 1296–1306. doi:10.1016/j.polymer.2014.01.035.

[20] L. Zhao, C. Wu, Z. Liu, Q. Zhang, X. Lu, Highly porous PVDF hollow fiber membranes for VMD application by applying a simultaneous co-extrusion spinning process, J. Memb. Sci. 505 (2016) 82–91. doi:10.1016/j.memsci.2016.01.014.

[21] K.W. Lawson, D.R. Lloyd, Membrane distillation. I. Module design and performance evaluation using vacuum membrane distillation, J. Memb. Sci. 120 (1996) 111–121. doi:10.1016/0376-7388(96)00140-8.

[22] Z.Q. Dong, X. hua Ma, Z.L. Xu, W.T. You, F. bing Li, Superhydrophobic PVDF-PTFE electrospun nanofibrous membranes for desalination by vacuum membrane distillation, Desalination. 347 (2014) 175–183. doi:10.1016/j.desal.2014.05.015.

[23] D. Sun, M.Q. Liu, J.H. Guo, J.Y. Zhang, B.B. Li, D.Y. Li, Preparation and characterization of PDMS-PVDF hydrophobic microporous membrane for membrane distillation, Desalination. 370 (2015) 63–71. doi:10.1016/j.desal.2015.05.017.

[24] D. Hou, J. Wang, X. Sun, Z. Ji, Z. Luan, Preparation and properties of PVDF

composite hollow fiber membranes for desalination through direct contact membrane distillation, J. Memb. Sci. 405–406 (2012) 185–200. doi:10.1016/j.memsci.2012.03.008.

[25] M. Baghbanzadeh, N. Hirceaga, D. Rana, T. Matsuura, C.Q. Lan, Effects of Polymer Ratio and Film-Penetration Time on the Properties and Performance of Nanocomposite PVDF Membranes in Membrane Distillation, Ind. Eng. Chem. Res. 55 (2016) 9971–9982. doi:10.1021/acs.iecr.6b02113.

[26] A. Alkhudhiri, N. Darwish, N. Hilal, Membrane distillation: A comprehensive review, Desalination. 287 (2012) 2–18. doi:10.1016/j.desal.2011.08.027.

[27] L.D. Tijing, Y.C. Woo, J.-S. Choi, S. Lee, S.-H. Kim, H.K. Shon, Fouling and its control in membrane distillation—A review, J. Memb. Sci. 475 (2015) 215–244. doi:10.1016/j.memsci.2014.09.042.

[28] D.M. Warsinger, J. Swaminathan, E. Guillen-Burrieza, H.A. Arafat, J.H. Lienhard V, Scaling and fouling in membrane distillation for desalination applications: A review, Desalination. 356 (2015) 294–313. doi:10.1016/j.desal.2014.06.031.

[29] L. Eykens, K. De Sitter, C. Dotremont, L. Pinoy, B. Van der Bruggen, Membrane synthesis for membrane distillation: A review, Sep. Purif. Technol. 182 (2017) 36–51. doi:10.1016/j.seppur.2017.03.035.

[30] L. Zhao, X. Lu, C. Wu, Q. Zhang, Flux enhancement in membrane distillation by incorporating AC particles into PVDF polymer matrix, J. Memb. Sci. 500 (2016) 46–54. doi:10.1016/j.memsci.2015.11.010.

[31] R.K. McGovern, J.H. Lienhard V, On the potential of forward osmosis to energetically outperform reverse osmosis desalination, J. Memb. Sci. 469 (2014) 245–250. doi:10.1016/j.memsci.2014.05.061.

[32] Y. Yang, D. Rana, T. Matsuura, C.Q. Lan, The heat and mass transfer of vacuum membrane distillation: Effect of active layer morphology with and without support material, Sep. Purif. Technol. 164 (2016) 56–62. doi:10.1016/j.seppur.2016.03.023.

[33] M. Khayet, Membranes and theoretical modeling of membrane distillation: A review, Adv. Colloid Interface Sci. 164 (2011) 56–88. doi:10.1016/j.cis.2010.09.005.

[34] J. Cai, X. Liu, Y. Zhao, F. Guo, Membrane desalination using surface fluorination treated electrospun polyacrylonitrile membranes with nonwoven structure and quasi-parallel fibrous structure, Desalination. 429 (2018) 70–75. doi:10.1016/j.desal.2017.12.019.

[35] J. Cai, F. Guo, Study of mass transfer coefficient in membrane desalination, Desalination. 407 (2017) 46–51. doi:10.1016/j.desal.2016.12.013.

[36] L. Wang, J. Min, Modeling and analyses of membrane osmotic distillation using non-equilibrium thermodynamics, J. Memb. Sci. 378 (2011) 462–470. doi:10.1016/j.memsci.2011.05.034.

[37] J.-G. Lee, W.-S. Kim, Numerical modeling of the vacuum membrane distillation process, Desalination. 331 (2013) 46–55. doi:10.1016/j.desal.2013.10.022.

[38] P. Onsekizoglu, K. Savas Bahceci, J. Acar, The use of factorial design for modeling membrane distillation, J. Memb. Sci. 349 (2010) 225–230. doi:10.1016/j.memsci.2009.11.049.

[39] R.W. Field, H.Y. Wu, J.J. Wu, Multiscale Modeling of Membrane Distillation: Some Theoretical Considerations, Ind. Eng. Chem. Res. 52 (2013) 8822–8828. doi:10.1021/ie302363e.

[40] A. Fick, On liquid diffusion, J. Memb. Sci. 100 (1995) 33–38. doi:10.1016/0376-7388(94)00230-V.

[41] N.A. Lange, J.G. Speight, Lange's handbook of chemistry., McGraw-Hill, 2005.

[42] B. Qi, B. Li, S. Wang, Investigation of Shell Side Heat Transfer in Cross-Flow Designed Vacuum Membrane Distillation Module, Ind. Eng. Chem. Res. 51 (2012) 11463–11472. doi:10.1021/ie203026b.

[43] S.K.S. Boetcher, Natural convection from circular cylinders, n.d.

[44] S. Bonyadi, T.S. Chung, Flux enhancement in membrane distillation by fabrication of dual layer hydrophilic-hydrophobic hollow fiber membranes, J. Memb. Sci. 306 (2007) 134–146. doi:10.1016/j.memsci.2007.08.034.

[45] R. Guha, B. Xiong, M. Geitner, T. Moore, T.K. Wood, D. Velegol, M. Kumar, Reactive micromixing eliminates fouling and concentration polarization in reverse osmosis membranes, J. Memb. Sci. 542 (2017) 8–17. doi:10.1016/j.memsci.2017.07.044.

[46] B. Kim, H. Kwon, S.H. Ko, G. Lim, J. Han, Partial desalination of hypersaline

brine by lab-scale ion concentration polarization device, Desalination. 412 (2017) 20–31. doi:10.1016/j.desal.2017.02.018.

[47] X. Su, W. Li, A. Palazzolo, S. Ahmed, Concentration polarization and permeate flux variation in a vibration enhanced reverse osmosis membrane module, Desalination. 433 (2018) 75–88. doi:10.1016/j.desal.2018.01.001.

[48] J. Heikkinen, H. Kyllönen, E. Järvelä, A. Grönroos, C.Y. Tang, Ultrasound-assisted forward osmosis for mitigating internal concentration polarization, J. Memb. Sci. 528 (2017) 147–154. doi:10.1016/j.memsci.2017.01.035.

[49] A.C. Sun, W. Kosar, Y. Zhang, X. Feng, A study of thermodynamics and kinetics pertinent to formation of PVDF membranes by phase inversion, Desalination. 309 (2013) 156–164. doi:10.1016/j.desal.2012.10.005.

[50] M.R. Qtaishat, T. Matsuura, Modelling of pore wetting in membrane distillation compared with pervaporation, in: Pervaporation, Vap. Permeat. Membr. Distill., Elsevier, 2015: pp. 385–413. doi:10.1016/B978-1-78242-246-4.00013-1.

Chapter 3

Synergic effects of hydrophilic and hydrophobic nanoparticles on performance of nanocomposite distillation membranes: An experimental and numerical study

Zhelun Li [a], Dipak Rana [a, *], Zhaohui Wang [b], Takeshi Matsuura [a], and Christopher Q. Lan [a, *]

[a] Department of Chemical and Biological Engineering, University of Ottawa, 161 Louis Pasteur Private, Ottawa, Ontario, K1N 6N5, Canada
[b] State Key Laboratory of Materials-Oriented Chemical Engineering, Nanjing Tech University, Nanjing, 210009, P.R. China

Separation and Purification Technology 202 (2018) 45–58

ABSTRACT

Supported flat sheet nanocomposite polyvinylidenefluoride (PVDF) membranes embedded with hydrophilic TiO_2, hydrophobic TiO_2, or the combination of them were fabricated via phase inversion process. The membranes were characterized by scanning electron microscopy, energy dispersive X-ray spectroscopy, atomic force spectroscopy, and the measurement of water contact angle and liquid entry pressure of water and subjected to tests on vacuum membrane distillation (VMD) performance. Addition of appropriate amounts of either hydrophilic or hydrophobic NPs was found to enhance VMD flux but hydrophilic NPs caused significant decrease of liquid entrance pressure of water (LEP_w) while hydrophobic particles did not show significant impacts on LEP_w. Addition of both hydrophilic and hydrophobic NPs demonstrated synergistic effects in terms of both enhanced flux and LEP_w due to their

different but complimentary effects on membrane structures. At feed temperature of 27.5℃, the VMD pure water permeate flux of the composite membrane embedded with 5 wt% hydrophilic TiO_2 NPs and 2 wt% of hydrophobic TiO_2 NPs (total 7 wt% NPs) was 4.26 kg/m^{2}h with a LEP_w of 28 psi, while those of neat PVDF membrane, the membrane embedded with 7 wt% of hydrophilic NP, and the membrane with 7 wt% hydrophobic nanoparticles were 0.335, 3.57, and 1.25 kg/m^{2}h, respectively and the LEPw of these membranes were 51, 24 and 47 psi, respectively. The salt rejection of above 99% could be maintained for 3 h by the membrane in which both hydrophilic and hydrophobic NPs were loaded. Numerical analyses of heat and mass transfer were also carried out to study the impact of hydrophilic and hydrophobic NPs on membrane characteristics.

Keywords: vacuum membrane distillation, nanocomposite membrane, nanoparticles, membrane structures

3.1 Introduction

Over the past few decades, desalination technology has attracted increasing attention from various fields, which is attributed to the fast-declining resources and rapid-increasing demand of fresh water. Several methods of removing salt from sea water have been devised, such as multiple effect distillation (MED), multi-stage flash distillation (MSF), mechanical vapor compression (MVC) and membrane separation, among which the membrane separation technology, with contribution to 63.7% of produced fresh water in the whole market, is now considered the dominant method in

desalination [1,2].

Membrane processes that are applicable to desalination include Reverse Osmosis (RO), Forward Osmosis (FO), and Membrane Distillation (MD), in which RO is currently the leading technology because of its low energy consumption, high permeability and technology maturity on a comparative basis [1,3]. However, RO has various and significant limitations, such as demand of high transmembrane pressure, highly sensitive to fouling and scaling, instability when dealing with high concentration brines and high electrical energy consumption[3–6]. MD process is an emerging technology, which is considered to have the capacity to rival RO processes in the near future, due to its potentials in providing high permeate flux at a low or near-zero transmembrane pressure, insensitivity to fouling, and ability to handle high concentration feed using low-grade or waste heat [3,7–10].

While extensive researches have demonstrated that the adding of nanoparticles can modify membrane structure and enhance membrane performance significantly in different membrane separation processes, studies on nanocomposite membranes for distillation are a relatively recent development and our research group has been playing a pioneering role in this field [11–16]. In our previous research, both hydrophobic and hydrophilic NPs were demonstrated to have a significant effect in enhancing membrane performance in MD processes[12–14]. Baghbanzadeh et al. [13] used hydrophilic CuO NPs as an additive in PVDF flat sheet membranes and applied

the made membrane in VMD process. A 153.4% increase in the flux was obtained at the feed temperature maintained at 27.5℃ when 2.0 wt% of CuO NPs were embedded in PVDF, and a growth of finger-like layer fraction with increasing NPs concentration in the composite membrane was also observed in the cross-section SEM images. In Efome et al. research[12], the performances of PVDF flat sheet membranes composited with superhydrophobic SiO_2 NPs in VMD process were investigated, and the experimental results showed that the VMD permeate flux of membrane with 7 wt% of hydrophobic SiO_2 NPs was nearly 4 times higher than that of neat PVDF membrane.

In this work, non-woven fiber (NWF) supported composite flat sheet PVDF membranes embedded with hydrophilic and hydrophobic TiO_2 NPs, individually or together, were fabricated by the phase inversion method using N,N-Dimethylacetamide(DMAc) and distilled water as solvent and non-solvent additive, respectively. Scanning electron microscopy (SEM) and atomic force microscopy (AFM) were carried out to characterize the membrane morphology, and the liquid entry pressure of water (LEPw), water contact angle, porosity, thickness and surface pore size distribution of the membranes were also measured. The membrane permeability and salt rejection performance were investigated by VMD experiment using pure water and artificial sea water as feed, respectively. This is the first time the effects of hydrophobic and hydrophilic nanoparticles on the properties and performance of distillation membranes are compared. Based on the results of these

experiments, which revealed the complimentary natures of these effects, the combination of hydrophilic and hydrophobic TO_2 nanoparticles are employed for fabrication of nanocomposite membranes and significant synergic effects were demonstrated.

3.2. Experimental materials and method

3.2.1 Materials

Two kinds of poly(vinylidene fluoride)(PVDF), Kynar®740 (Pellet, $M_W = 410kDa$) and Kynar® HSV900 (Powder,$M_W = 1548kDa$) kindly supplied by Arkema Inc. (Philadelphia, PA) were used in this experiment as host polymers. Anhydrous *N,N*-dimethylacetamide(DMAc) with the purity of 99.8% was purchased from Sigma-Aldrich Inc. (St. Louis, MO). Hydrophilic TiO_2 NPs were purchased from Ishihara Sangyo Kaisha Ltd.(Osaka, Japan) while the silicon-coated hydrophobic TiO_2 NPs were supplied by Skyspring Nanomaterials Inc. (Houston, TX). The particle size of hydrophilic and hydrophobic TiO_2 NPs are 20nm and 10-30nm, respectively. Non-woven polyester fiber, Hollytex® 3396, used as backing material was supplied by Kavon Filter Products Co. (Farmingdale, NJ). The air permeability of the backing material is 0.009 cubic feet per minute per square meter (CFM). The tensile strength and the elongation of the material are 85 lb/in and 75 % in the machine direction, respectively, while those in the cross direction are 52 lb/in and 85 %. Sodium chloride and n-butanol were purchased from Fisher Scientific (Fair Lawn, NJ). All chemicals were used as received.

3.2.2 Membrane fabrication

Phase inversion method was used in this experiment to fabricate the membranes. First, 15 wt.% of PVDF (HSV900:740=2:8), 1.25 wt.% of water and 83.75 wt.% of DMAc were mixed together under stirring at 180rpm and 50℃ for 72h to make the dope solution. The desired type and amount of TiO_2 NPs were added after the dope solution was degassed under room temperature for 24 h. The resulting mixtures were then allowed to be stirred by an over-head stirrer and degassed under vacuum for 2h and 1h, respectively, before it was cast by a casting bar (250 μm thickness) on the NWF backing materials using uniform-speed automatic film applicator (model AFA-II, Beijing, China). The cast film was immersed in distillate water at 25℃ along with the backing material to induce phase inversion process after exposing to air for around 1 min. Thereafter, the membranes were kept in the water bath for 24h while the water was replaced every 6 h to make sure the solvent DMAc was removed completely. The membranes were then dried at room temperature for 24h to be ready for the following test. The membrane codes are given according to the dope compositions in Table 3-1.

Table 3-1
Composition of the dope solution for nanocomposite membrane preparation.

Membrane code[a]	Dope solution concentration (wt%)			Concentration of NPs x (wt%) added to (100-x) wt% of dope solution	
	PVDF	DMAc	Water	Hydrophilic TiO_2	Hydrophobic TiO_2
M-0	15	83.75	1.25	0.0	0.0
M-L2	15	83.75	1.25	2.0	-

M-L4	15	83.75	1.25	4.0	
M-L5	15	83.75	1.25	5.0	
M-L7	15	83.75	1.25	7.0	
M-L9	15	83.75	1.25	9.0	
M-B2	15	83.75	1.25	-	2.0
M-B5	15	83.75	1.25	-	5.0
M-B7	15	83.75	1.25	-	7.0
M-L2-B2	15	83.75	1.25	2.0	2.0
M-L3.5-B3.5[b]	15	83.75	1.25	3.5	3.5
M-L5-B2	15	83.75	1.25	5.0	2.0

[a] L and B are for hydrophilic and hydrophobic NPs respectively. The number after L and B indicates the weight percent of NP added to the balance of dope solution.

[b] This membrane dope solution was prepared for viscosity measurements only.

3.2.3 Characterization of dope solution

A rotational rheometer (Brookfield, Synchro-Lectric viscometer model: LVF) was used to measure the viscosity of the dope suspension with different types and amounts of TiO_2 NPs. An appropriate spindle was chosen and three different motor speeds were applied to measure the suspension viscosity. Three viscosity measurements were performed at each of the three difference speeds, and the average value was reported.

3.2.4 Membrane characterization

3.2.4.1 Cross-sectional membrane structure

Cross-section structure of membrane samples was observed by SEM. And a further detailed SEM mapping of sponge-like layer was also performed to analyze its structural change. The membrane sample was immersed in liquid nitrogen for approximately 10 seconds and then broken before it was supplied to the SEM equipment (S-4800, Hitachi) to avoid membrane bending during the observation.

Nanomaterial distribution within the membrane layer was examined using an

energy dispersive X-ray (EDX) analyzer. The samples were gold sputtered before they were applied to the instrument. (Oxford Inca Energy 250X EDX)

Membrane thickness was measured using a digital micrometer measure at different spots for at least 10 times, and the average value was calculated.

Porosity measurement of membrane samples was carried out by applying the wet and dry method. The weight of membrane sample was measured (w_1), after it was immersed in n-butanol for at least 12h to ensure that the sample was completely wetted by the liquid. The sample was then dried in an oven for 24h at 50℃ to ensure the complete evaporation of liquid, followed by weighing (w_2). The equation below was used to calculate the porosity of sample:

$$\%\varepsilon = \frac{w_1 - w_2}{A.l.\rho} \times 100\% \quad (1)$$

Where ε is the membrane porosity (%), A is the membrane surface area (cm^2), l is the thickness (cm), ρ is the n-butanol density (g/cm^3). Three measurements were carried out and the average value was reported.

3.2.4.2 Top-surface features

Pore size of membrane top surface was analyzed using ImageJ software based on its top-surface SEM images. At least ten randomly selected areas in three different SEM

images of each membrane sample were examined and the average values and standard deviations of mean pore size, pore size distribution and surface porosity were presented.

Water contact angle was measured using a VCA Optima Surface Analysis System (AST Product, Inc. Billerica, MA) to evaluate the membrane surface hydrophobicity. A 1μL of deionized water was dropped by a micro pipette (Hamilton Company, Reno, NV) on the membrane surface, followed by the measurement of contact angle after a 10s waiting. Ten randomly selected spots of each of three different coupons taken from a membrane sheet were tested, and the average value is reported.

Roughness of membrane surface was visualized and investigated using an atomic force microscope (AFM) Park XE-100 (Park Systems, South Korea) and the 3-D surface morphology of prepared membranes and different surface roughness parameters were obtained.

3.2.5 Membrane performance

3.2.5.1 Vacuum membrane distillation (VMD)

The VMD performance of membranes was investigated by a still column VMD setup which we used in our previous research[12,17,18]. The membrane sample was mounted in the cell which was filled with either distilled or sodium chloride solution, and vacuum was applied on the permeate side to facilitate vapor transfer. A heating

tape connected to a temperature controller was wrapped around the static cell to maintain the feed temperature at 27.5℃, while a magnetic stirrer was equipped inside the feed chamber to minimize the effect of temperature and concentration polarization. The condenser was cooled by liquid nitrogen to make sure all permeate vapor was condensed. The VMD permeate flux was calculated by the following equation:

$$J = \frac{w}{A.t} \qquad (2)$$

Where J is the permeate flux of the membrane (kg/m^2.h), w is the weight of collected permeate (kg) during time t (h), and A is the effective membrane area (m^2). For each membrane, VMD experiments were repeated six times, and the average flux value was calculated to narrow the error range. A more detailed description of this process can be found in our previous work[14].

3.2.5.2 Liquid entry pressure of water (LEPw)

The setup with a detailed diagram shown in our previous work was used to measure the LEPw of the membranes[12,17,18]. The membrane sample was fixed in the static cell loaded with distillate water in the feed chamber at ambient temperature. Pressure supplied by compressed nitrogen from a cylinder was applied on the feed side liquid and increased gradually by a regulator at an interval of 0.14 bar (2 psi). The pressure was kept constant for 10min at each pressure, and the pressure at which the first droplet was observed at the permeate outlet of cell was recorded as LEPw. The

measurement was repeated three times for each type of membrane and the average value was calculated and reported.

3.2.5.3 Rejection

To investigate the rejection performance of the membrane, artificial seawater (35g sodium chloride per liter of water) was used as the feed in the VMD setup and a conductivity meter (OAKTON, CON 2700) was utilized to measure the conductivities of feed (C_f), condensate (C_p) and deionized water (C_d). The following equation was employed to get the salt rejection (R):

$$\%R = \frac{C_f - C_p}{C_f - C_d} \times 100 \qquad (3)$$

3.3 Results and discussion

3.3.1 Viscosity

The experimental data for viscosity is presented in Fig. 3-1. In the figure, the concentration of M-L-B indicates the total concentration including both hydrophilic TiO_2 nanoparticles (L) and hydrophobic TiO_2 nanoparticles (B). For example, the concentration of M-L5-B2 is 7 wt.% (i.e., 5% L plus 2% B). (The same rule is applied in all the following data plots.) The figure illustrates a gradual growth trend in viscosity with an increase of NP concentration for all three series of dopes (M-L, M-B and M-L-B), with M-B showing the most remarkable increase. The growth of

suspension viscosity with the increase of NP concentration could be attributed to the increase in the aggregation of NPs in the suspension, and as a consequence the increase in the NP aggregate size. The highest viscosity of M-B is due to the enhanced aggregation of hydrophobic TiO_2 NPs in polar DMAc solvent. As well, the viscosity of M-L3.5-B3.5 dope was higher than M-L5-B2, which further confirmed that the hydrophobic TiO_2 NP contributes more to the viscosity enhancement.

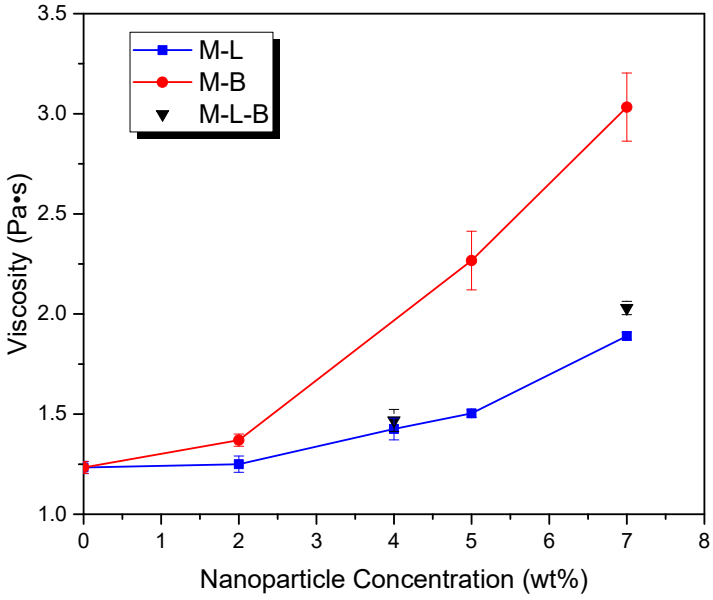

Fig. 3-1. Viscosity values of the various dope solutions

3.3.2 Morphology

3.3.2.1 SEM

The SEM images of the top-surface, the total cross-section and the sponge-like layer with higher magnification are shown in Fig. 3-2a, b and c, respectively, for M-L, M-B,

M0 and M-L-B membranes. ImageJ was then used to analyze the SEM images. Figures 3-3, 3-4, and 3-5 show the surface porosity, the average pore size, the cumulative pore size distribution, as a result of ImageJ analysis, among which the surface porosity was defined as the ratio of pore area to the total membrane area within a top surface SEM image and cumulative pore size distribution is the ratio of cumulative area of the pores whose diameters are smaller than a specific value to the total pore area by assuming that all the pores could be seen as circle.

In Fig. 3-2a, the number of pores at the top-surface increased significantly with an increase in NP concentration both for M-L and M-B series. This could be explained by the delayed demixing caused by increasing viscosity, which promotes the separation of polymer-rich and polymer-poor phases and thus more pores would be formed at the top-surface of the membrane[19–22]. This explanation can also be justified by the observation that M-B membranes with higher viscosities have larger number of pores than M-L membranes.

In Fig. 3-3 remarkable increase in the surface porosity with an increase in NP concentration is observed for both M-L and M-B. In Fig. 3-4 the pore size of M-L also increases remarkably. In contrast, the pore size remains almost constant for M-B. The surface porosity increase of M-B is therefore primarily due to the increase in the number of pores.

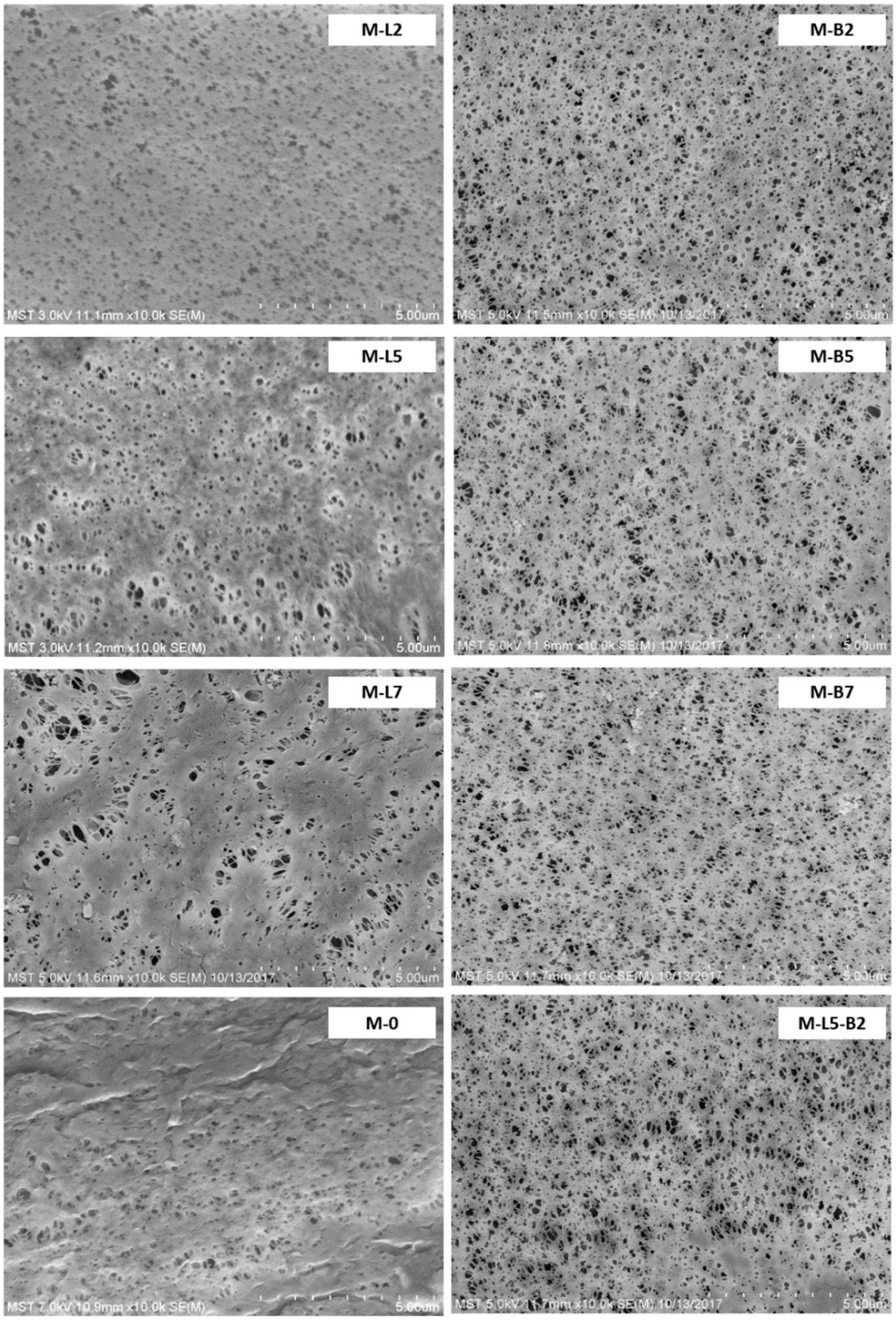

Fig. 3-2a SEM image of the flat sheet membranes at the top surface

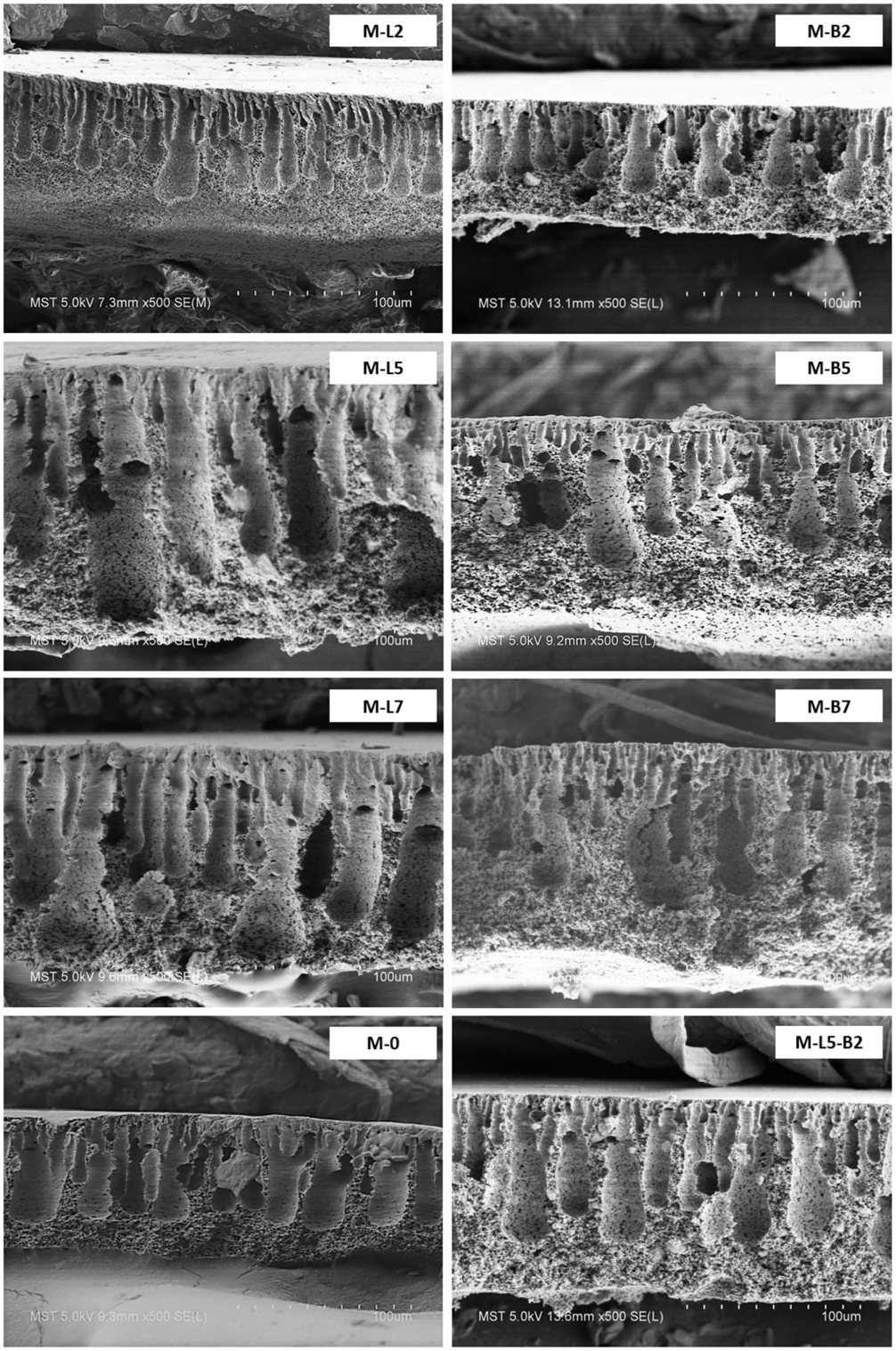

Fig. 3-2b Cross-sectional SEM images of the flat sheet membranes

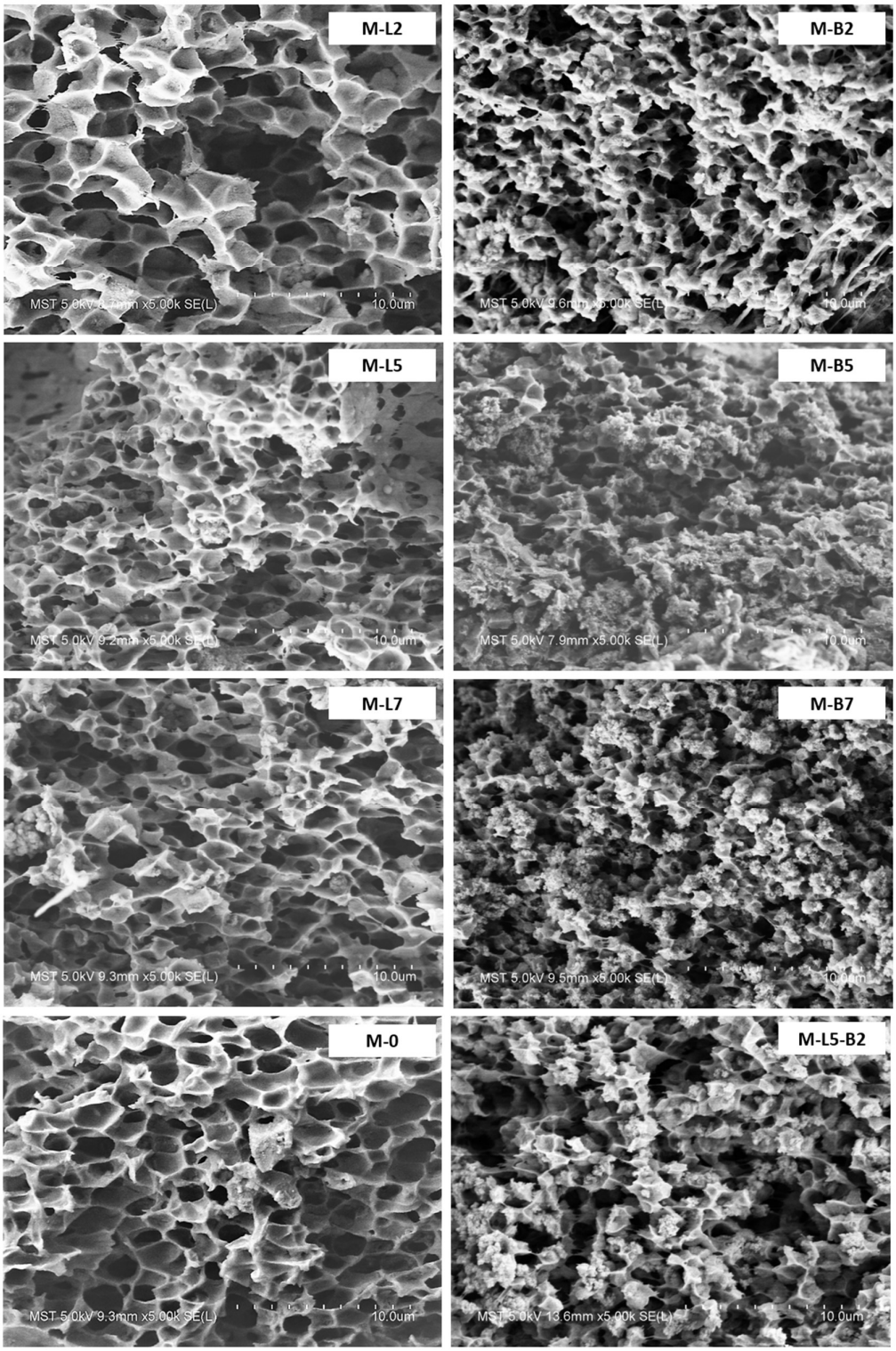

Fig. 3-2c SEM images of the sponge-like layer with higher magnification

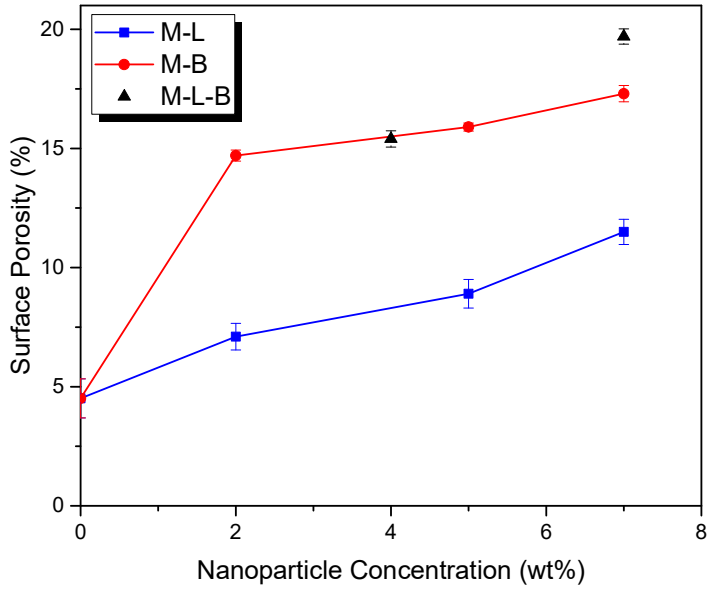

Fig. 3-3. Effect of NPs type and concentration on surface porosity

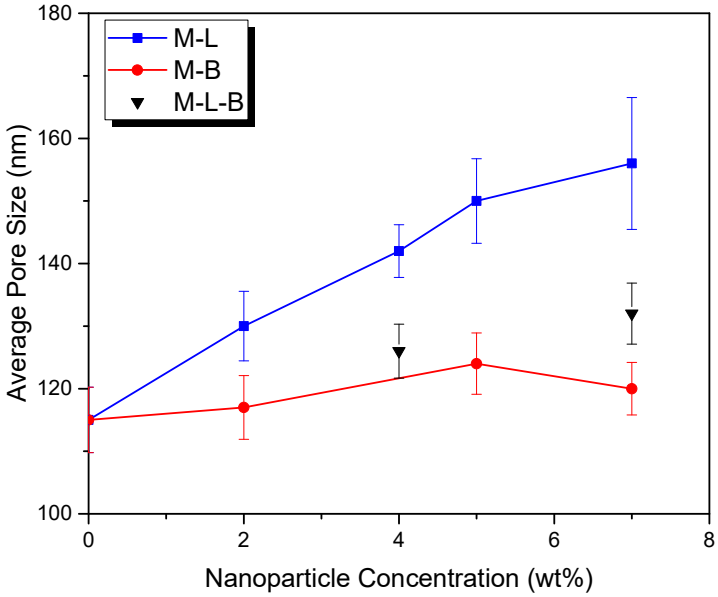

Fig. 3-4. Effect of NPs type and concentration on average pore size

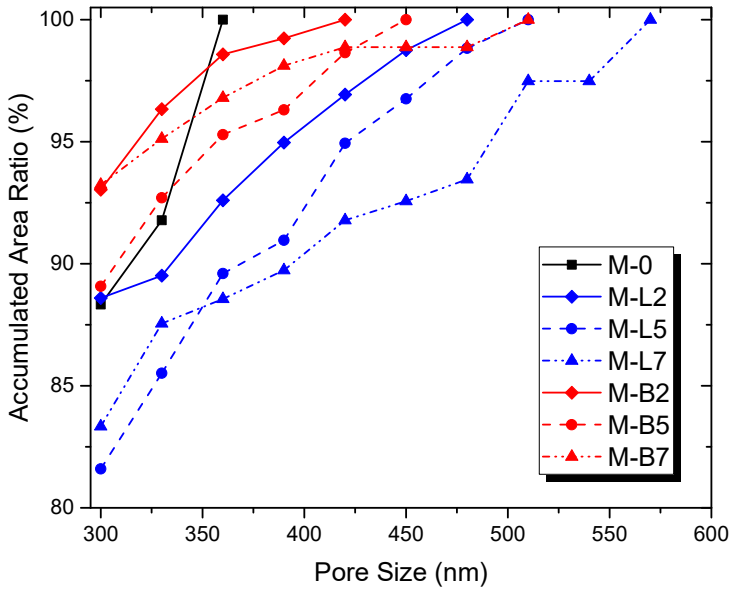

Fig. 3-5. Cumulative pore size distribution of the membranes

The details of the pore size distribution are illustrated in Fig. 3-5. Large shifts of the pore size distribution toward right (larger pore size) is detected for M-L due to the hydrophilic property of NP, while the shift of M-B is much less.

Figures 3-6 and 3-7 show the finger-like layer ratio (defined as the ratio of finger-like layer area to the total area of the membrane cross-section) obtained from the cross-sectional images in Fig. 3-2c and the bulk porosity, respectively. It should be noted that both are the bulk properties of the membranes. It should also be noted that the boundary between the finger-like and sponge-like layer became less distinguishable at the high hydrophilic NP concentration.

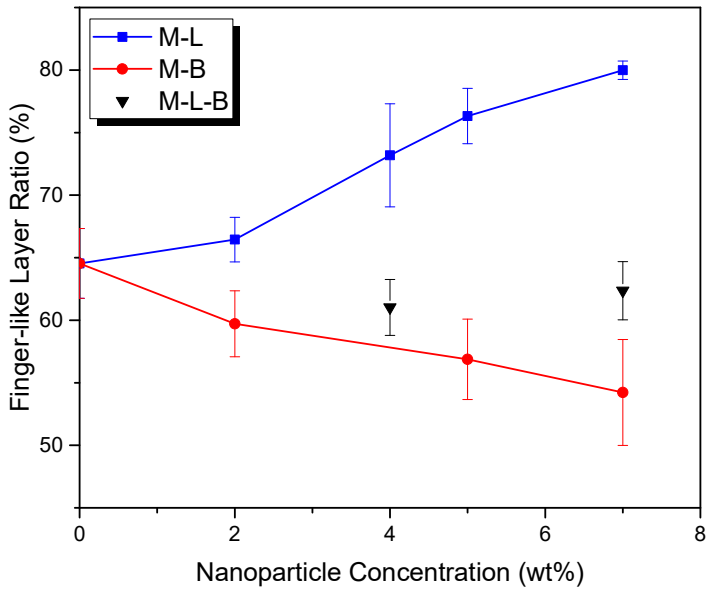

Fig. 3-6. Effect of NPs type and concentration on finger-like layer ratio

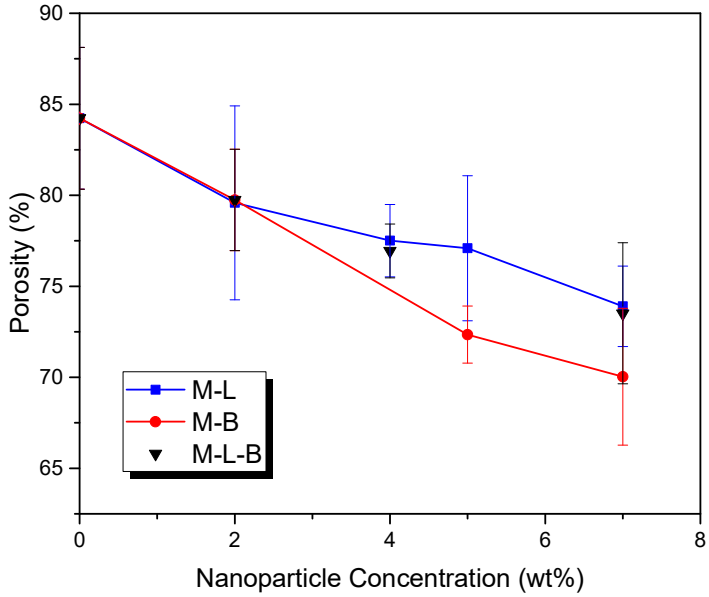

Fig. 3-7. Effect of NPs type and concentration on membrane bulk porosity

In Fig. 3-6 the finger-like layer ratio of M-L increases remarkably, indicating that hydrophilic NPs draw water deep into the membrane. In contrast, the ratio decreases

for M-B, indicating hydrophobic NPs prevent penetration of water.

Interestingly, the bulk porosity of the membrane decreases for both M-L and M-B. The porosity decrease is understandable for M-B but the result was rather surprising for M-L. This is because the finger-like void space became narrower as the rate of nonsolvent(water)/solvent (DMAc) is slowed down considerably with an increase in dope viscosity [21,23]. A magnified image of the sponge-like layer in Fig. 3-2c shows that hydrophilic NP in M-L has no obvious impact on sponge-like layer morphology. However, a large amount of agglomerated NPs are found in the sponge-like macro-voids of M-B due to the enhanced agglomeration of hydrophobic NPs, as already mentioned.

3.3.2.2 Particle distribution

A typical EDX spectrum of M-L5-B2 shown in Fig. 3-8 indicates the presence of silicon and titanium in the membrane. Silicone is from the coated layer of hydrophobic NPs. Figures 3-9a and b show the EDX mappings for the cross-section and the top surface, respectively. Both Figs. 3-9a and b demonstrate the uniform distribution of the elements in the space occupied by PVDF. Bright masses in the TiO_2 mapping represent the agglomerated NPs. Similar spectra and elemental mapping were obtained for the other membranes.

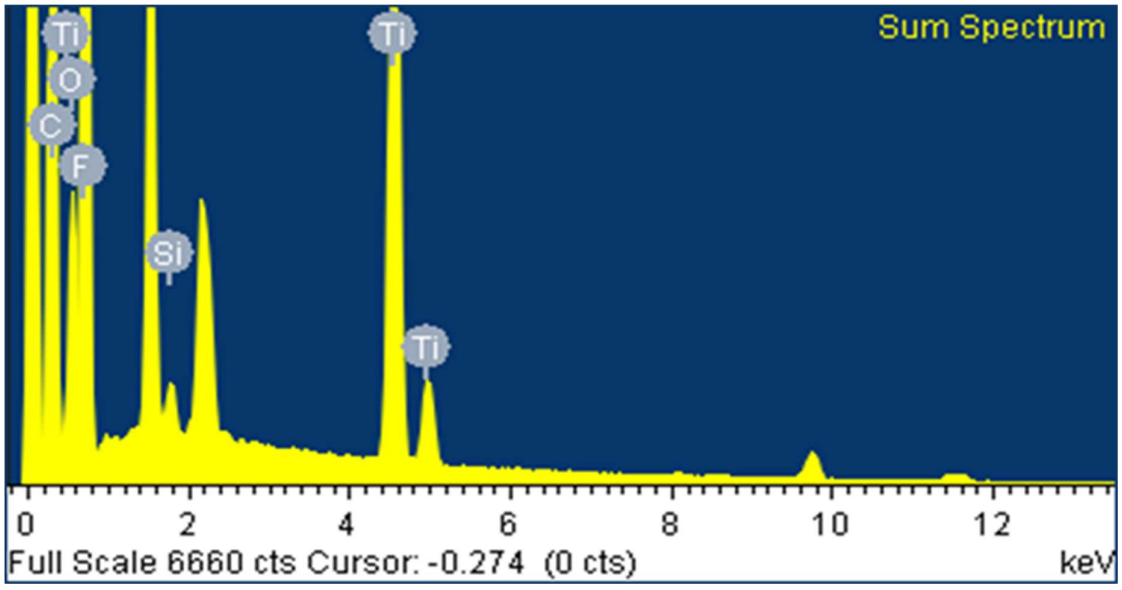

Fig. 3-8. EDX image of nanocomposite membrane M-L5-B2

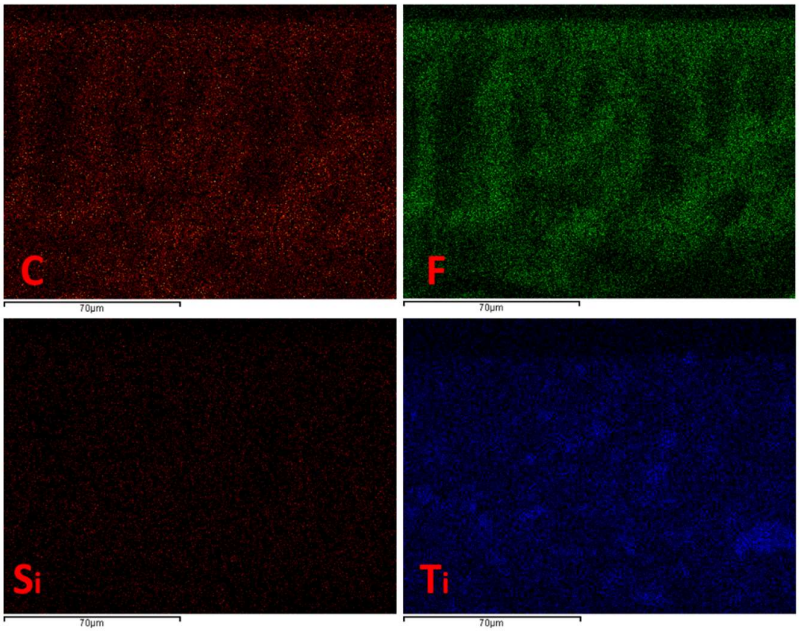

(a)

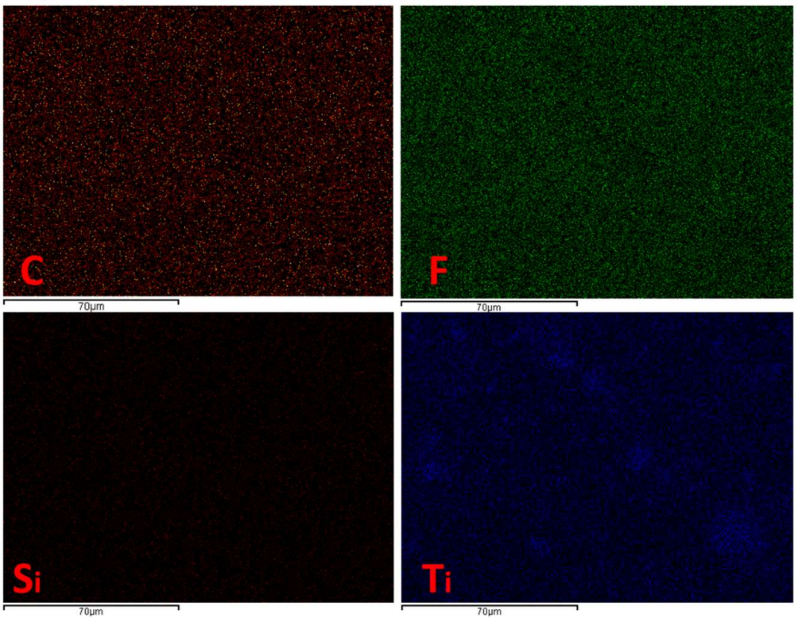

(b)

Fig. 3-9. EDS mapping of C, F, Si and Ti for M-L5-B2.
(a) cross-section, and (b) top-surface

3.3.2.3 Roughness (AFM)

Typical 3-D surface images are shown in Fig. 3-10 while the roughness parameters for all the membranes are given in Table 3-2. As one can observe, incorporation of both hydrophilic and hydrophobic TiO_2 NPs increased the surface roughness.

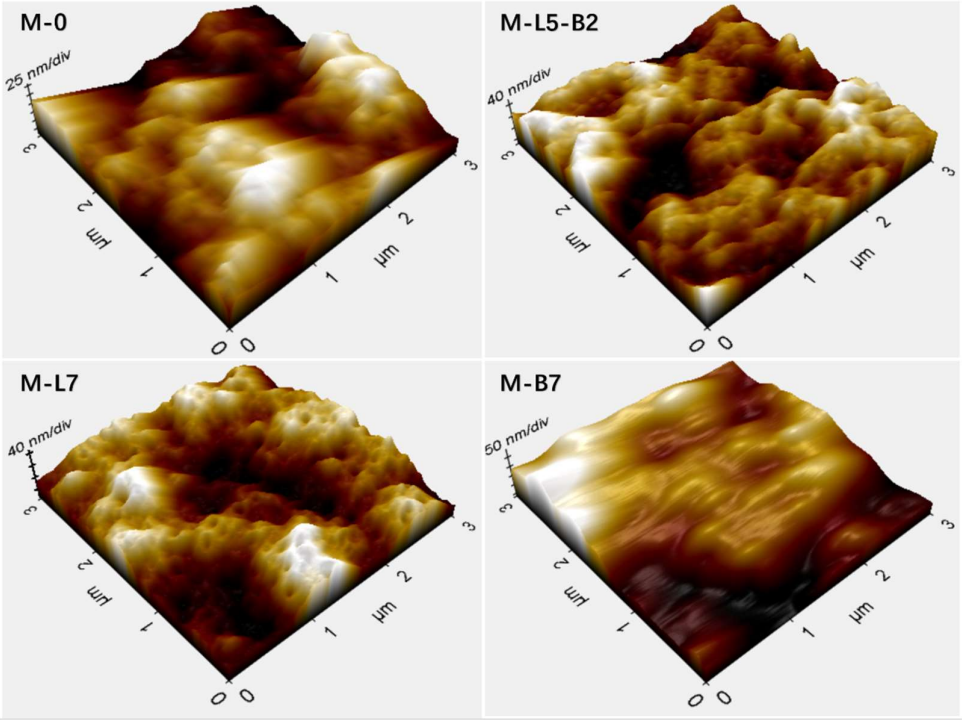

Fig. 3-10. AFM image of M-0.M-L5-B2, M-L7 and M-B7 membranes

Table 3- 2
Surface roughness of prepared nanocomposite membranes.

Membrane label	R_a (nm) [a]	R_q (nm) [b]	R_{max} (nm) [c]
M-0	26.22	33.17	207.90
M-L2	27.79	35.81	234.57
M-L5	32.47	41.02	281.40
M-L7	33.08	43.50	298.73
M-B2	29.37	43.03	256.97
M-B5	33.65	45.79	304.76
M-B7	34.17	46.26	320.09
M-L5-B2	32.62	41.60	283.95

[a] R_a: Arithmetical mean deviation

[b] R_q: Root mean square deviation

[c] R_{max}: Vertical distance between highest peak and lowest valley

3.3.2.4 Contact angle

The results of the water contact angle measurement are summarized in Fig. 3-11. From Fig.3-11, the increase of statistical significance was observed for the contact angle of M-B, while the change was insignificant for M-L. For M-B, the increase of water contact angle could be attributed to the increase of surface roughness and the hydrophobicity of the NPs while the insignificant contact angel change of M-L could be explained by the compromise between the increase of surface roughness and hydrophilicity of the NPs.

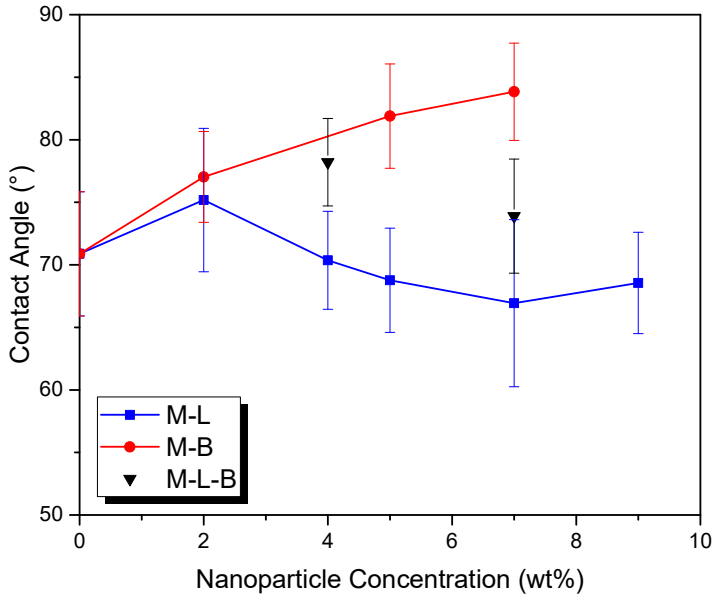

Fig. 3-11. Effect of NPs type and concentration on water contact angle.

3.3.3 Performance analysis of M-L and M-B membranes

3.3.3.1 LEPw

The results of the LEPw measurement are summarized in Fig. 3-12. The LEPw of M-L membranes decreases steeply with an increase in NP concentration, which parallels the increase of the average surface pore size, shown in Fig.3-4. Particularly, the increase in the large pores (Fig. 3-5) contributed significantly to the decrease of LEPw. On the other hand, the LEPw of M-B decreases slightly by the particle loading of 0 to 5wt%, and then levels off, which is attributed to a slight increase of the average pore size (Fig. 3-4) and the counter-effect of the slight increase in contact angle (Fig. 3-11).

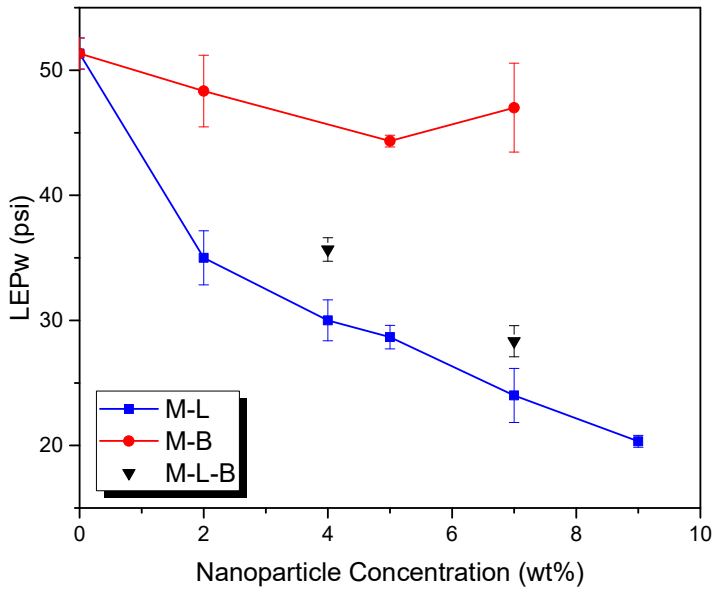

Fig. 3-12. Effect of NPs type and concentration on LEPw.

3.3.3.2 Flux

Pure water fluxes of M-L, M-B and M-L-B membranes are given as a function of NPs concentration in Fig. 3-13. According to Fig. 3-13, the pure water permeate flux increases upon addition of fillers for all M-L, M-B and M-L-B. The flux of M-L increases steeply from 0 to 5wt% and then levels off, which corresponds to the simultaneous increase of the finger-like layer ratio (Fig. 3-6) and the surface porosity (Fig. 3-3). On the other hand, the flux of M-B initially increases from 0 to 2 wt.% faster than M-L, but quickly levels off thereafter. This could be attributed to the initial increase of surface porosity that is faster than M-L (Fig. 3-3), which is later compromised by the decrease in the finger-like layer ratio (Fig. 3-6). Table 3-3 shows the effects of the concentration of hydrophilic and hydrophobic NPs on the performance and morphology of nanocomposite membranes studied in this work together with the works done in the past. As shown in Table 3-3, the flux, the finger-like layer ratio and the average pore size increase, whereas LEPw decreases with an increase in NP concentration. The trends are the same for hydrophobic NPs when the NP concentrations are low. With a further increase of the NP concentration the trend is reversed.

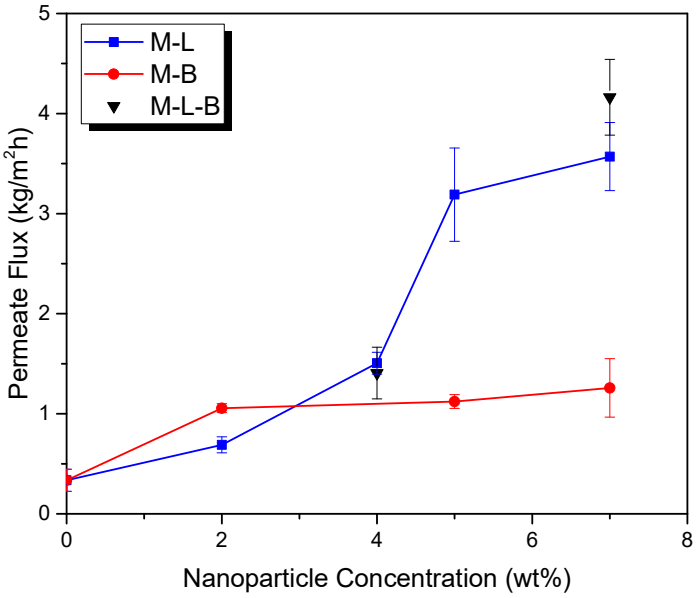

Fig. 3-13. Effect of NPs type and concentration on pure water permeate flux

Table 3-3
Trends in the performance and morphology of nanocomposite VMD membranes with an increase in the concentration of hydrophilic ad hydrophobic NPs.

Particle Type	Nanoparticle	Performance		Morphology		Reference
		Flux	LEPw	Finger-like layer ratio	Average pore size	
Hydrophilic	SiO_2	+	-	+	+~	[14]
	CuO	+~	-~	+	+~	[13]
	TiO_2	+[a]	-	+	+	[this work]
Hydrophobic	SiO_2	+~	-~	-	+-	[12]

$CaCO_3$	+-	-~	-	+-	[16]
TiO_2	+~	-~	-	+-	[this work]

[a] + means increase, - means decrease, +~ means increase at low particle concentration and then level off, -~ means decrease at low particle concentration and then level off, +- means increase at low particle concentration and decrease at high particle concentration

3.3.4 Performance enhancement via hydrophilic and hydrophobic nanoparticles cooperation

Referring to the mixing of hydrophilic and hydrophobic NPs, it should be reminded that on the M-L-B line 4 wt.% means M-L2-B2 and 7wt.% means M-L5-B2. Now we compare the effect of the addition of hydrophilic and hydrophobic NPs at the higher end of the total NPs concentration. Addition of 2 wt.% of hydrophilic particle from M-L5 to M-L7causes only a marginal increase of flux from 3.2 to 3.5 kg/m^{2}h while the addition of 2wt% of hydrophobic NP from M-L5 to M-L5-B2 results in more remarkable increase to 4.256 kg/m^2 h. The reason for this synergistic effect of hydrophilic and hydrophobic NPs is primarily due to the surface porosity increase from M-L5 to M-L5-B2 (see Fig. 3), which surpasses the increase from M-L5 to M-L7.

As listed in Table 3-4, the VMD permeate flux enhancement via different optimization methods for PVDF membrane were compared, and the significant improvement produced by hydrophilic and hydrophobic NPs can be clearly demonstrated.

Table 3-4
Comparation of different PVDF membranes optimization methods in term of VMD permeate flux enhancement

Optimization Strategy	Feed conditions	Pure water flux before optimization (kg/m^2h)	Pure water flux after optimization (kg/m^2h)	Increasement of flux	Reference

Surface Modification （Facile bio-inspired mineralization）	Pure water, 60℃	~10.0	~11.0	~10.0%	[24]
	Pure water, 80℃	~28.0	~29.5	~5.4%	
Blending of different PVDF polymers (Different molecular weight)	Pure water, Room temperature	~13.9	~26.2	~88.5%	[25]
	3.5% NaCl aqueous, Room temperature	~12.7	~22.1	~74.0%	
Optimization of membrane fabrication (co-extrusion spinning)	Pure water, 70℃	~37.5	~61.8	~64.8%	[26]
Addition of macro-size particles (Activated carbon)	10% NaCl aqueous, 70℃	~20.7	~26.9	~30.0%	[27]
Cooperation with another polymer material (PDMS)	2.0% NaCl aqueous, 50℃	~9.6	~15.2	~58.3%	[28]
Cooperation with another polymer material (PTFE)	Pure water, 60℃	~16.7	~18.4	~10.2%	[29]
Addition of hydrophilic NPs (SiO_2)	Pure water, 27.5℃	~0.5	~12.7	~2456.0%	[14]
Addition of hydrophobic NPs (Surface modified SiO_2)	Pure water, 27.5℃	~0.7	~2.9	~292.4%	[12]
Additions of both hydrophilic and hydrophobic NPs (hydrophilic and hydrophobic TiO_2)	Pure water, 27.5℃	~0.3	~4.3	~1333.3%	[this work]

3.3.5 Rejection

VMD experiments were carried out with synthetic seawater as feed using M-L5-B2 which showed the highest flux among all the studied membranes. The salt rejection during the operation period of 3 h is presented in Fig. 3-14. The salt rejection over 99.9% could be maintained during the entire period of operation, which indicates a good and stable salt rejection performance, despite the low contact angle of the membrane.

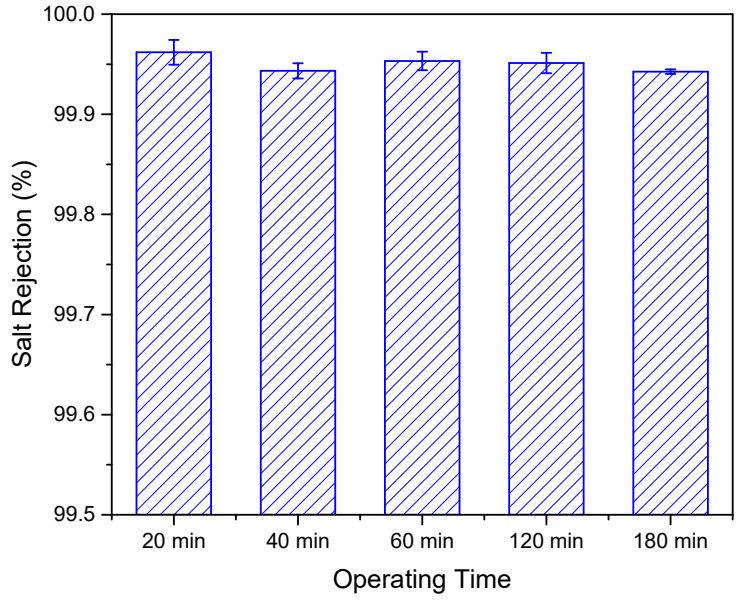

Fig. 3-14. Salt rejection vs. operating time for M-L5-B2 membrane

3.4. Numerical analysis of the process

3.4.1 Heat transfer

The heat transfer process of VMD consists of three paths, which are the feed bulk to the feed side membrane surface, feed side membrane surface to that of permeate side,

permeate side membrane surface to the cold trap surface. However, the heat conduction from permeate side membrane surface to the cold trap surface is too low to be considered due to low pressure which is close to a vacuum.

For the heat transfer from feed bulk to the membrane surface at feed side, the heat flux is given by:

$$Q_f = h_f(T_{bf} - T_{mf}) \tag{4}$$

where $Q_f(W/m^2)$ is the heat flux from feed bulk to the membrane surface at feed side through the liquid boundary layer, T_{bf} and T_{mf} are temperatures of feed bulk and feed side membrane surface, respectively. $h_f(W/m^2\,K)$ is the heat transfer coefficient which can be calculated using Nusselt number (N_u)[30]:

$$h_f = \frac{N_u k}{L_c} \tag{5}$$

where L_c (m) and k (W/mK) are the characteristic length and the fluid thermal conductivity, respectively. N_u can be obtained by:

$$N_u = 0.53(P_r \cdot G_r)^{0.25} \text{ when } 10^3 < P_r \cdot G_r < 10^6 \tag{6-a}$$

$$N_u = 0.13(P_r \cdot G_r)^{0.33} \text{ when } 10^6 < P_r \cdot G_r < 10^{12} \tag{6-b}$$

where Prandtl number, P_r ,and Grashof number, G_r, are given as:

$$P_r = \frac{\mu C_p}{k} \tag{7}$$

$$G_r = \frac{L_c^3 \rho^2 \beta g (T_{bf} - T_{mf})}{\mu^2} \tag{8}$$

where μ (Pa s), C_p (J/kgK), ρ (kg/m^3), β $(1/K)$ are viscosity, heat capacity, density, volume thermal expansion of the feed water at given temperature,

respectively, and g is the gravitational acceleration (9.8 m/s^2).

For the heat transfer process through the membrane (from the feed side membrane surface to the permeate side membrane surface), the heat flux is given as:

$$Q_m = J_m \Delta H_{evap} \tag{9}$$

where Q_m (W/m^2) and J_m (kg/m^2 s) are the heat and mass flux through the membrane, respectively, and ΔH_{evap} (kJ/kg) is the enthalpy of evaporation of water at the given temperature.

Furthermore, the heat flux through the whole VMD system, Q_{total} (W/m^2), is given as:

$$Q_{total} = Q_f = Q_m \tag{10}$$

And to further detect the effect of membrane types and feed temperatures on heat transfer of VMD process, the temperature polarization coefficient (TPC) is defined as [31]:

$$\text{TPC} = \frac{T_{mf}}{T_{bf}} \tag{11}$$

The values of parameters required above are listed in Table 3-5. The temperature of membrane surface at feed side, T_{mf}, was computed via Excel Solver by setting $Q_f = Q_m$ and TPC was further calculated by equation 11. The results of TPC are shown in Fig. 15, although TPCs exhibited slight decreasing trends with an increase in the temperature, they were nearly equal to unity, which is a characteristic feature of VMD.

Table 3-5

Property of water (liquid) at different temperatures.

Parameter	Unit	Values at different temperatures		
		27.5℃	40℃	50℃
C_p	J/kg K	4179	4179	4179
μ	Pa s	0.00084	0.00065	0.00055
k	W/m K	0.608	0.627	0.641
ρ	kg/m^3	995	989	981
g	m/s^2	9.8	9.8	9.8
L_c	m	0.17	0.17	0.17
β	1/K	0.00029	0.000385	0.000458
ΔH_{evap}	kJ/kg	2436.6	2406.9	2382.9

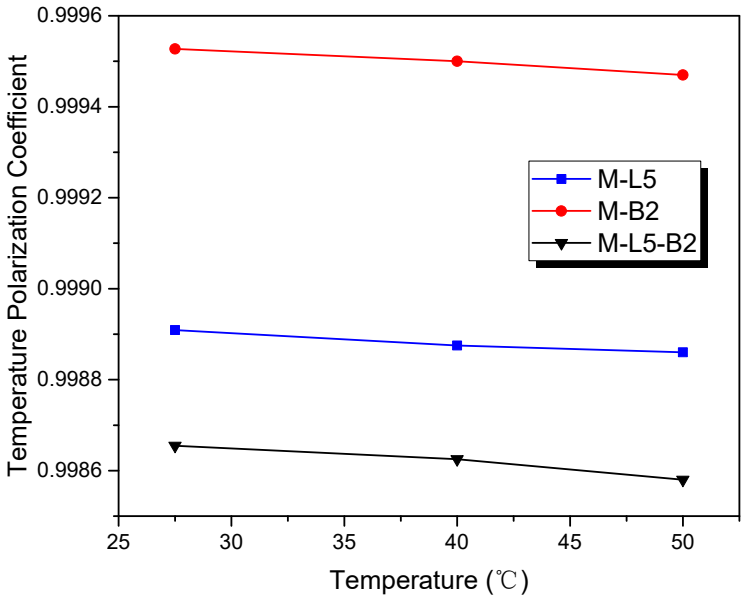

Fig. 3-15. Effect of feed temperature on TPC for M-L5, M-B2, M-L5-B2 membranes

3.4.2 Mass transfer

Membrane distillation is a thermal driven process with the driving force being the difference between the saturation pressure at the feed side membrane surface (p_{mf}, Pa) and the vapour pressure at the permeate side membrane surface (p_{mp}, Pa). The flux (J, kg/m^2 S) is given by the following equation derived based on the Fick's law [32]:

$$J = K_m(p_{mf} - p_{mp}) \quad (12)$$

where K_m is the mass transfer coefficient of vapour across the membrane.

For VMD, p_{mp} is the absolute pressure on the permeate side and p_{mf} is dependent on the water temperature at feed side membrane surface (T_{mf}, K), which could be calculated based on the Antoine equation [33]

$$p_{mf}(T_{mf}) = \exp(23.1964 - \frac{3816.44}{T_{mf} - 46.13}) \quad (13)$$

The VMD fluxes of M-L5 and M-B2 at different temperatures were measured and the results together with those of M-L5-B2 are listed in Table 6. The mean free path (λ) was calculated to be $6.5 - 8.5 \times 10^{-7} m$ under the experimental conditions of this work and the majority of the pore diameters are between 0.1λ and 100λ, hence both Knudsen and the viscous flow may occur. Therefore, the mass transfer coefficient can be given as

$$K_m = K_{knudsen} + K_{viscous} = \frac{2}{3}\frac{r\varepsilon}{\tau\delta}\sqrt{\frac{8M}{\pi RT}} + \frac{r^2\varepsilon M p}{8\tau\delta\mu RT} \quad (14)$$

where $r\ (m), \varepsilon(-), \tau(-),\ \delta$(m), μ (Pa s) are membrane pore radius, porosity, pore tortuosity, membrane thickness and the water vapor viscosity, respectively. M (18.02 kg/kmol) is the water molecular weight and R (8.314 x 10^3 J/kmol K) is the molar gas constant.

Further by comparing $K_{knudsen}$and $K_{viscous}$numerically under the experimental conditions and with the parameters given in Table 4, $K_{viscous}$ is orders of magnitude smaller than $K_{knudsen}$ and hence can be ignored. Then Equation 14 is reduced to,

$$K_m = K_{knudsen} = \frac{2}{3}\frac{r\varepsilon}{\tau\delta}\sqrt{\frac{8M}{\pi RT}} \quad (15)$$

As r, ε, δ are all measured experimentally, the pore tortuosity, τ, can be calculated, and the results at 27.5℃ are shown in Fig. 3-16, The figure shows that the adding of both hydrophilic and hydrophobic NPs can decrease pore tortuosity to reduce the mass transfer resistance through the membranes.

Table 3- 6
Pure water flux of M-L5-B2, M-L5, M-B2 at different temperatures.

Membrane label	M-L5-B2			M-L5			M-B2		
Temperature (℃)	27.5	40	50	27.5	40	50	27.5	40	50
Permeate flux (kg/m^2h)	4.26 ±0.42	8.40 ±1.05	13.50 ±1.273	3.19 ±0.29	6.31 ±0.92	9.91 ±1.13	1.06 ±0.09	2.11 ±0.13	3.29 ±0.18

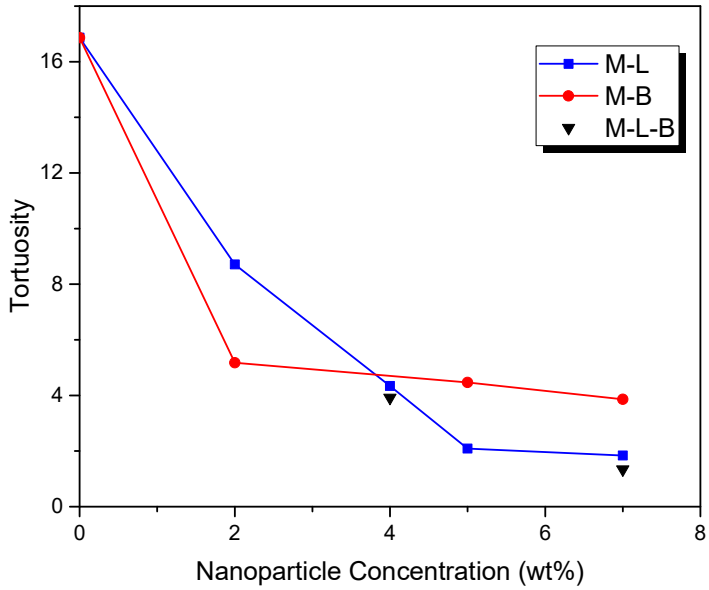

Fig. 3-16. Effect of NPs type and concentration on membrane pore tortuosity

3.4.3 Effect of operating temperature

The pure water permeate fluxes of membrane M-L5-B2 at different feed temperatures are presented in Fig. 3-17. The flux at feed temperature of 27.5℃ was used as the base value to calculate the tortuosity of membranes, which is then used in Equation 14 for determination of K_m and then Equation 12 for calculation of J at 40 and 50℃. As depicted in Fig. 3-17, the experimental fluxes at 40 and 50°C matched well with the calculated fluxes at corresponding temperatures.

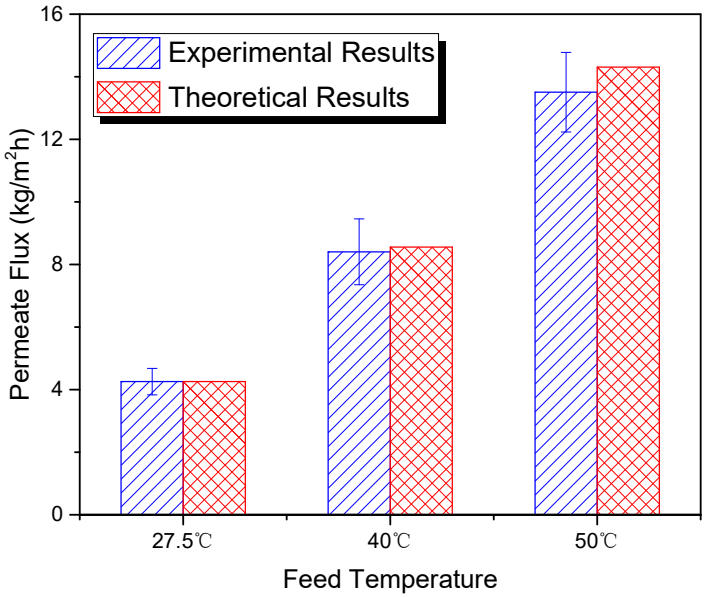

Fig. 3-17. Effect of feed temperature on permeate flux for M-L5-B2 membrane

3.5 Conclusion

In this study, supported PVDF membranes incorporated with hydrophilic and hydrophobic TiO_2 NPs separately or together were fabricated by the phase inversion process. The membranes were characterized by SEM, EDX, AFM, and LEPw and contact angle measurement. The membranes were further tested for their performance

by VMD experiments. The following conclusions can be drawn from this study:

1) Both hydrophilic and hydrophobic NPs could enhance the membrane performance in VMD process.

2) Incorporation of the hydrophilic NPs facilitates the deeper penetration of finger-like macro-voids, and enlarges the membrane surface pore size, both of which contribute to increase of flux. However, enlargement of finger-like layer may decrease the mechanical strength while increase of pore size reduces LEPw.

3) Incorporation of the hydrophobic NPs can shorten the finger-like macro-voids and make membrane denser while increasing the number of surface pores and the surface porosity, the latter two factors are the major contributors leading to increased flux.

4) When hydrophobic NPs are added to the membrane of high hydrophilic NP content (M-L5), the increase in flux is more than the further addition of hydrophilic NPs. This is primarily due to the increase in surface porosity by the addition of hydrophobic NPs, which surpasses the increase in surface porosity by the hydrophilic NPs.

5) TPC decreases slightly with the increment of membrane permeate flux and feed bulk temperature but is nearly equal to unity.

6) Mass transfer through the prepared membranes is dominated by the Knudsen diffusion and both hydrophilic and hydrophobic NPs caused decrease of pore tortuosity.

7) Pure water flux of the membrane loaded with 5wt% and 2wt% of hydrophilic

and hydrophobic TiO_2 NPs, respectively, could reach 4.256 kg/m^{2}h at feed temperature of 27.5℃. The latter flux is 1142% higher than that of the neat PVDF membrane. This is the result of the synergistic effect of hydrophilic and hydrophobic NPs on the membrane flux, i.e. 1) At 5 wt% addition, the flux of hydrophilic NP (M-L5) is 3 times higher than the hydrophobic NP (M-B5). 2) By adding another 2 wt% of NP, flux increment by hydrophobic NP (M-L5-B2) is 3.5 ((4.256–3.2)/(3.5-3.2)) times higher than hydrophilic NP (M-L7). Thus, both effects combined, the highest flux was achieved by M-L5-B2.

Despite the synergistic effect, the flux reported in this work is low compared to those reported in the literature. This can be attributed to the feed temperature as low as 27.5^{o}C.

Moreover, salt rejection over 99.9% was maintained during VMD of 3 h by this membrane.

Acknowledgements

The authors are thankful for the kind gift of the polymers (Kynar® 740 and Kynar® HSV900) by Arkema Inc. (Philadelphia, PA, U.S.A.). Financial supports from the NSERC Discovery and I2I grants are also highly appreciated.

Reference

[1] N. Ghaffour, T.M. Missimer, G.L. Amy, Technical review and evaluation of

the economics of water desalination: Current and future challenges for better water supply sustainability, Desalination. 309 (2013) 197–207. doi:10.1016/j.desal.2012.10.015.
[2] J. Yin, B. Deng, Polymer-matrix nanocomposite membranes for water treatment, J. Memb. Sci. 479 (2015) 256–275. doi:10.1016/j.memsci.2014.11.019.
[3] A.S. Hassan, H.E.S. Fath, Review and assessment of the newly developed MD for desalination processes, Desalin. Water Treat. 51 (2013) 574–585. doi:10.1080/19443994.2012.697273.
[4] T.H. Chong, S.L. Loo, A.G. Fane, W.B. Krantz, Energy-efficient reverse osmosis desalination: Effect of retentate recycle and pump and energy recovery device efficiencies, Desalination. 366 (2015) 15–31. doi:10.1016/j.desal.2015.01.017.
[5] R.K. McGovern, J.H. Lienhard V, On the potential of forward osmosis to energetically outperform reverse osmosis desalination, J. Memb. Sci. 469 (2014) 245–250. doi:10.1016/j.memsci.2014.05.061.
[6] L. Karimi, L. Abkar, M. Aghajani, A. Ghassemi, Technical feasibility comparison of off-grid PV-EDR and PV-RO desalination systems via their energy consumption, Sep. Purif. Technol. 151 (2015) 82–94. doi:10.1016/j.seppur.2015.07.023.
[7] M.A.E.R. Abu-Zeid, Y. Zhang, H. Dong, L. Zhang, H.L. Chen, L. Hou, A comprehensive review of vacuum membrane distillation technique, Desalination. 356 (2015) 1–14. doi:10.1016/j.desal.2014.10.033.
[8] J.G. Lee, Y.D. Kim, W.S. Kim, L. Francis, G. Amy, N. Ghaffour, Performance modeling of direct contact membrane distillation (DCMD) seawater desalination process using a commercial composite membrane, J. Memb. Sci. 478 (2015) 85–95. doi:10.1016/j.memsci.2014.12.053.
[9] G. Guan, X. Yang, R. Wang, A.G. Fane, Evaluation of heat utilization in membrane distillation desalination system integrated with heat recovery, Desalination. 366 (2015) 80–93. doi:10.1016/j.desal.2015.01.013.
[10] W.G. Shim, K. He, S. Gray, I.S. Moon, Solar energy assisted direct contact membrane distillation (DCMD) process for seawater desalination, Sep. Purif. Technol. 143 (2015) 94–104. doi:10.1016/j.seppur.2015.01.028.
[11] M. Baghbanzadeh, D. Rana, C.Q. Lan, T. Matsuura, Effects of Inorganic Nano-Additives on Properties and Performance of Polymeric Membranes in Water Treatment, Sep. Purif. Rev. 45 (2016) 141–167. doi:10.1080/15422119.2015.1068806.
[12] J.E. Efome, M. Baghbanzadeh, D. Rana, T. Matsuura, C.Q. Lan, Effects of superhydrophobic SiO<inf>2</inf> nanoparticles on the performance of PVDF flat sheet membranes for vacuum membrane distillation, Desalination. 373 (2015) 47–57. doi:10.1016/j.desal.2015.07.002.
[13] M. Baghbanzadeh, D. Rana, T. Matsuura, C.Q. Lan, Effects of hydrophilic CuO nanoparticles on properties and performance of PVDF VMD membranes, Desalination. 369 (2015) 75–84. doi:10.1016/j.desal.2015.04.032.

[14] M. Baghbanzadeh, D. Rana, C.Q. Lan, T. Matsuura, Effects of hydrophilic silica nanoparticles and backing material in improving the structure and performance of VMD PVDF membranes, Sep. Purif. Technol. 157 (2016) 60–71. doi:10.1016/j.seppur.2015.11.029.
[15] D. Hou, J. Wang, X. Sun, Z. Ji, Z. Luan, Preparation and properties of PVDF composite hollow fiber membranes for desalination through direct contact membrane distillation, J. Memb. Sci. 405–406 (2012) 185–200. doi:10.1016/j.memsci.2012.03.008.
[16] D. Hou, G. Dai, H. Fan, J. Wang, C. Zhao, H. Huang, Effects of calcium carbonate nano-particles on the properties of PVDF/nonwoven fabric flat-sheet composite membranes for direct contact membrane distillation, Desalination. 347 (2014) 25–33. doi:10.1016/j.desal.2014.05.028.
[17] Y. Yang, D. Rana, T. Matsuura, S. Zheng, C.Q. Lan, Criteria for the selection of a support material to fabricate coated membranes for a life support device, RSC Adv. 4 (2014) 38711–38717. doi:10.1039/C4RA04638B.
[18] Z. Chen, D. Rana, T. Matsuura, Y. Yang, C.Q. Lan, Study on the structure and vacuum membrane distillation performance of PVDF composite membranes: I. Influence of blending, Sep. Purif. Technol. 133 (2014) 303–312. doi:10.1016/j.seppur.2014.07.015.
[19] C.A. Smolders, A.J. Reuvers, R.M. Boom, I.M. Wienk, Microstructures in phase-inversion membranes. Part 1. Formation of macrovoids, J. Memb. Sci. 73 (1992) 259–275. doi:10.1016/0376-7388(92)80134-6.
[20] S. Bonyadi, T.S. Chung, Flux enhancement in membrane distillation by fabrication of dual layer hydrophilic-hydrophobic hollow fiber membranes, J. Memb. Sci. 306 (2007) 134–146. doi:10.1016/j.memsci.2007.08.034.
[21] C.K. Chiam, R. Sarbatly, Vacuum membrane distillation processes for aqueous solution treatment-A review, Chem. Eng. Process. Process Intensif. 74 (2014) 27–54. doi:10.1016/j.cep.2013.10.002.
[22] Z. Chen, D. Rana, T. Matsuura, D. Meng, C.Q. Lan, Study on structure and vacuum membrane distillation performance of pvdf membranes: II. influence of molecular weight, Chem. Eng. J. 276 (2015) 174–184. doi:10.1016/j.cej.2015.04.030.
[23] H. Fan, Y. Peng, Application of PVDF membranes in desalination and comparison of the VMD and DCMD processes, Chem. Eng. Sci. 79 (2012) 94–102. doi:10.1016/j.ces.2012.05.052.
[24] W. Zhong, J. Hou, H.C. Yang, V. Chen, Superhydrophobic membranes via facile bio-inspired mineralization for vacuum membrane distillation, J. Memb. Sci. 540 (2017) 98–107. doi:10.1016/j.memsci.2017.06.033.
[25] A. Figoli, S. Simone, A. Criscuoli, S.A. Al-Jlil, F.S. Al Shabouna, H.S. Al-Romaih, E. Di Nicolò, O.A. Al-Harbi, E. Drioli, Hollow fibers for seawater desalination from blends of PVDF with different molecular weights: Morphology, properties and VMD performance, Polym. (United Kingdom). 55 (2014) 1296–1306. doi:10.1016/j.polymer.2014.01.035.
[26] L. Zhao, C. Wu, Z. Liu, Q. Zhang, X. Lu, Highly porous PVDF hollow fiber

membranes for VMD application by applying a simultaneous co-extrusion spinning process, J. Memb. Sci. 505 (2016) 82–91. doi:10.1016/j.memsci.2016.01.014.
[27] L. Zhao, X. Lu, C. Wu, Q. Zhang, Flux enhancement in membrane distillation by incorporating AC particles into PVDF polymer matrix, J. Memb. Sci. 500 (2016) 46–54. doi:10.1016/j.memsci.2015.11.010.
[28] D. Sun, M.Q. Liu, J.H. Guo, J.Y. Zhang, B.B. Li, D.Y. Li, Preparation and characterization of PDMS-PVDF hydrophobic microporous membrane for membrane distillation, Desalination. 370 (2015) 63–71. doi:10.1016/j.desal.2015.05.017.
[29] Z.Q. Dong, X. hua Ma, Z.L. Xu, W.T. You, F. bing Li, Superhydrophobic PVDF-PTFE electrospun nanofibrous membranes for desalination by vacuum membrane distillation, Desalination. 347 (2014) 175–183. doi:10.1016/j.desal.2014.05.015.
[30] S.K.S. Boetcher, Natural convection from circular cylinders, n.d.
[31] Y. Yang, D. Rana, T. Matsuura, C.Q. Lan, The heat and mass transfer of vacuum membrane distillation: Effect of active layer morphology with and without support material, Sep. Purif. Technol. 164 (2016) 56–62. doi:10.1016/j.seppur.2016.03.023.
[32] A. Fick, On liquid diffusion, J. Memb. Sci. 100 (1995) 33–38. doi:10.1016/0376-7388(94)00230-V.
[33] N.A. Lange, J.G. Speight, Lange's handbook of chemistry., McGraw-Hill, 2005.

Chapter 4

Fabrication and VMD Performance of Flat Sheet PVDF-PTFE Composite Membranes

Zhelun Li, Dipak Rana, Takeshi Matsuura, Christopher Q. Lan

Department of Chemical and Biological Engineering, University of Ottawa, 161 Louis Pasteur Private, Ottawa, Ontario, K1N 6N5, Canada

Abstract

Supported flat sheet PVDF-PTFE composite membranes were fabricated for the first time using phase inversion process in this study. The prepared composite membranes were characterized by SEM, ATR-FTIR and water contact angle measurements and LEPw, they were then subjected to VMD experiments. Addition of appropriate amounts of PTFE was demonstrated to have great potential in enhancing permeate flux of PVDF membranes while maintain an acceptable LEPw value. At feed temperature of 30℃, the VMD pure water permeate flux of the prepared composite membrane embedded with 40 wt% PTFE (membrane code: M-40) was 5.61 kg/m^{2}h, while that of pure PVDF membrane was 0.71 kg/m^{2}h. The salt rejection of the prepared composite membranes were all above 99.5%, which indicates the applicability of the PVDF-PTFE composite membranes in desalination.

4.1 Introduction

Fresh water shortage has been recognized as one of the major challenges and in the coming future, because of the fast depletion of ground water. It has been claimed that around 1.8 billion people from all over the world would suffer absolute water scarcity by 2025[1,2]. However, nearly 97% of all the earth's water is sea water which has not been utilized sufficiently, and as a result, desalination technology, considered as an effective way to solve fresh water crisis, is attracting more and more attentions over the past few decades.

An emerging sea water purification method, membrane distillation (MD), has been considered as the promising next-generation desalination technology because of its advantages when compared with the frequent-utilized desalination methods such as reverse osmosis (RO) and forward osmosis (FO). These include: (1) low energy consumption and ability to use low quality thermal energy; (2) ability to handle highly concentrated saline water feed; (3) high quality of produced water; and (4) mild operation conditions.[1,3–10]

Various hydrophobic polymer materials are utilized for MD membrane fabrication, such as polyvinylidene fluoride (PVDF), polytetrafluoroethylene (PTFE) and polypropylene (PP), among which PVDF is the most frequent-used material currently due to its excellent mechanical strength and chemical resistance, outstanding dispersity in organic solvents (like N, N-dimethylacetamide (DMAC)) and ease in fabrication.

On the other hand, PTFE has the lowest surface energy which demonstrated the highest hydrophobicity[11]. A contact angel at 139.81° can be achieved by the PTFE flat-sheet membranes made by Huang [12], meanwhile the contact angle of pure PVDF flat-sheet membranes is only 125° tested by Razmjou [13]. Furthermore, the excellent thermal resistance, extremely high chemical stability and low surface friction of PTFE makes it famous as "the King of Plastic" and PTFE was also recognized as the prime polymer material for MD membrane fabrication because of these features. However, another fact is, PTFE is also famous for its tough-handle processing property and most of the current membrane fabrication methods, like phase inversion method and melt spinning method, are not suitable for this material. Various methods for PTFE membrane fabrication have already been proposed in the last decades, however, nearly all of them require high temperature environment which makes the fabrication process uneconomical.

Table 4-1
Comparation of PVDF and PTFE.

Materials	PVDF	PTFE
Full name	Poly(vinylidene fluoride)	Poly(tetrafluoroethylene)
Formula	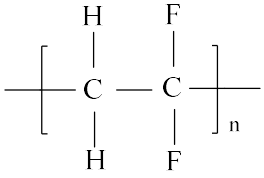	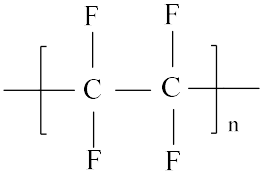
Hydrophobicity	Lower	Higher
Dispersity in organic solvents (e.g. DMAc)	Easy	Hard

Membrane fabrication ability	Easy	Hard

Thus, an attempt was made to fabricate PVDF-PTFE composite membranes which would not only have the excellent properties of PTFE but could be fabricated as easy as PVDF membranes. In this work, the PVDF-PTFE flat sheet membranes were fabricated the first time by phase inversion method and introduced to VMD process for desalination purposes. The product membranes were made by the phase inversion method using DMAC as the sovent and water as the non-solution. The support material, non-woven fiber, was applied to make the membranes more durable for the VMD process. Several characterization techniques were used to characterize the prepared membranes, such as scanning electron microscope (SEM), attenuated total reflectance (ATR)-Fourier transformed infrared spectroscopy (FTIR), water contact angle (CA). The membrane performance are evaluated in forms of the liquid entry pressure of water (LEPw), salt rejection and VMD permeate flux.

4.2 Experimental

4.2.1 Materials

Polyvinylidene fluoride (PVDF) pellets, Kynar® 740, were kindly supplied by Arkema Inc. (Philadelphia, PA) while polytetrafluoroethylene (PTFE) powder (with an average particle size of 2-3 μm) was purchased from MicroLubrol. Anhydrous N,N-

dimethylacetamide (DMAc, 99.8%) used as the disperse solvent was supplied by Sigma-Aldrich Inc. (St. Louis, MO). The backing material, non-woven polyester fiber Hollytex® 3396, was purchased from Kavon Filter Products Co. (Farmingdale, NJ). Sodium chloride used for artificial sea water preparation and n-butanol used for membrane porosity measurement were supplied by Fisher Scientific (Fair Lawn, NJ). All chemicals above were used as received.

4.2.2 Dope solution preparation

As PTFE is hard to be dispersed in dope solutions due to its extreme hydrophobicity, the dispersion of PTFE in DMAc was prepared first through a harsh process. Specific amounts of PTFE powder were added into DMAc solvent and the obtained solution was then applied to magnetic agitation under high temperature for 2 hours to make sure the surface of PTFE powder was completely wetted by the solvent, before a 3-hour long ultrasonication process was carried out to efficiently separate the aggregated PTFE particles (set amplitude as 85 Hz, pulse-on time as 10 second, pulse-off time as 15 second). Then, desired amounts of PVDF pellets and distilled water were mixed into the prepared well-dispersed PTFE-DMAc solution (As shown in Fig.4-1) and the mixture were shaken for at least 48 hours using a thermos shaker under 50℃ until the homogeneous dope solution was obtained.

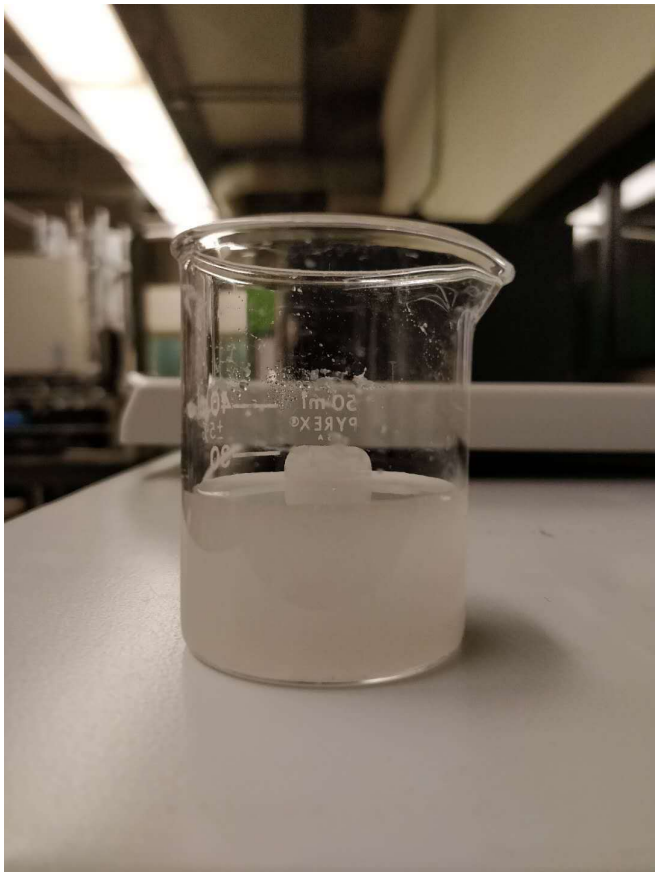

Fig.4-1 Prepared well-dispersed PTFE-DMAc solution

4.2.3 PVDF-PTFE blended membrane fabrication

Phase inversion method was used in this study to prepare the non-woven fiber supported flat sheet membranes. A steel casting bar (casting thickness 250μm) attached to a uniform-speed automatic film applicator (model AFA-II, Beijing, China) was utilized to cast the resultant dope solution into a film on the non-woven fiber backing material. The cast film was exposed to air for 15s-30s before it immersed into 25℃ distilled water together with the backing material letting the membrane formed via phase inversion process. Before the testing, the prepared membranes were allowed to dry in

air for at least 24 hours after a 24-hour long distilled water bath immersion which would guarantee the complete removal of solvent DMAc. The fabricated membranes were coded according to the weight concentrations of PTFE materials in the total polymers, and the code are shown in Table. 4-2.

Table 4-2
Composition of the dope solution for PVDF-PTFE composite membrane preparation.

Membrane Code	PTFE loading in the membrane (wt%)	Component ratios in the dope solution
M-0	0	The ratio of PVDF/DMAc/Distilled Water≡ 15/83.75/1.25
M-5	5	
M-10	10	
M-20	20	
M-30	30	
M-40	40	
M-50	50	

4.2.4 Membrane performance experiments

4.2.4.1 Liquid entry pressure of water (LEP w)

The LEPw value of the prepared membrane was detected by a setup which was described detailly in our previous work[14–17]. A cell connected with a feed chamber filled with distilled water was utilized to clamp the membrane sample, and pressure supplied by compressed nitrogen gas cylinder was applied at the top of feed chamber

to induce the osmosis of the feed water through the membrane sample. The pressure applied was increased step wise using a valve at an intervals of 2 psi for every 10 mins. The pressure showed on the compressed gas cylinder gauge when the first droplet of water was detected at permeate outlet of the cell was recorded as the LEPw value of the tested membrane sample. Three LEPw tests were carried out for each type of membrane and the average value was calculated and reported.

4.2.4.2 Permeate flux and salt rejection in vacuum membrane distillation (VMD)

The VMD experiments were carried out by a setup which was used in our previous work[14–18]. The membrane sample was fixed in a cylindrical permeation cell with a feed chamber contains pure water or artificial seawater. The feed chamber was wrapped by a heating tape which connected with a temperature controller, so that the feed temperature can be adjusted as needed. A nearly vacuum environment was created by a vacuum pump at the permeate side to induce the permeation of the evaporative water and liquid nitrogen was also applied to condense the permeate vapor.

For pure water permeate flux test, the feed temperature was maintained at 30℃. And the flux was calculated according to:

$$J = \frac{w}{A \cdot t} \quad (1)$$

Where J, w, A, t are the permeate flux of the membrane (kg/m^{2}h), weight of collected

water (kg), effective membrane area (m^2), experimental time (h). For each type of prepared membranes, the pure water permeate flux test was taken for at least 6 times and the average value was reported.

In term of artificial seawater permeate flux and salt rejection detections, the experiments were carried out at three different feed temperatures (30℃, 40℃ and 50℃). For each membrane type tested, the salt rejection was obtained from:

$$\%R = \frac{C_f - C_p}{C_f - C_d} \times 100 \quad (2)$$

Where C_f, C_p, C_d represent the conductivities of feed, condensate and deionized water measured by a conductivity meter (OAKTON, CON 2700), respectively. And the artificial seawater was prepared based on the ratio of 35g sodium chloride per liter of water.

4.2.5 Membrane characterizations

4.2.5.1 Scanning electron microscope (SEM)

Characterization on the morphology of membrane top surfaces and cross-sections was performed by SEM (Vega-II XMU VPSEM and Anatech Hummer VII) imaging. To get a unconvoluted cross-sectional image, the membrane samples were broken carefully after an immersion in liquid nitrogen for around 15s. Furthermore, all samples were sputtered by gold prior to the SEM analysis.

4.2.5.2 SEM image analysis

The software ImageJ was utilized to analysis the top surface and cross-sectional SEM images. The average pore size and surface porosity can be obtained from top surface image while the finger-like layer ratio can be obtained based on cross-sectional image. During the analysis for top surface SEM images, the detected pores whose areas are smaller than 500nm^2 were ignored to decrease the impacts of image noise points.

4.2.5.3 ATR-FTIR analysis

Attenuated total reflectance (ATR)-Fourier transformed infrared spectroscopy (FTIR) detection was carried out to analysis the top surface contents of the prepared membrane using the Agilent tech-Cary 630 (Agilent, Canada) spectrometer. The membrane samples were dried well before were pressed and fixed on the prism ready for the test.

4.2.5.4 Membrane porosity

Wet and dry method was applied to measure the porosity of the membrane sample. The top layer of the tested membrane sample was firstly peeled off from the support material and then immersed in n-butanol for 12h to make sure that the sample was sufficiently padded. The weight of the wetted sample was measured and marked as w_1 before the sample was dried in an oven overnight at 50℃ to ensure that the n-butanol was completely evaporated from the membrane sample. The weight of the dried sample was marked as w_2. The porosity of the membrane sample was then obtained by the

following equation:

$$\%\varepsilon = \frac{w_1 - w_2}{A.l.\rho} \times 100\% \quad (3)$$

Where ε, A, l, ρ are the membrane porosity (%), membrane surface area ($c\,m^2$), membrane thickness (cm) and density of n-butanol (g/cm^3), respectively. Three measurements were taken for each type of membrane samples, and the average result calculated.

4.2.5.5 Water contact angel (CA)

VCA Optima Surface Analysis System (AST Product, Inc. Billerica, MA) was utilized to measure the water contact angle of the membrane sample. Each measurement was carried out after waiting for 10 seconds after a droplet of deionized water, which is 1μL, was dropped on the membrane surface utilizing a micro pipette (Hamilton Company, Reno, NV). The contact angle of 30 randomly selected spots was measured for each membrane sample and the average and error values were calculated and reported.

4.3 Results and Discussion

4.3.1 SEM

Fig. 4-2a and Fig.4-2b show the SEM images for the prepared membranes in term of

top surface and cross-section, respectively. And Fig.4-3 shows the average pore size and surface porosity analyzing results given by a picture analyzing software ImageJ, the using details of which can be found in our previous work.

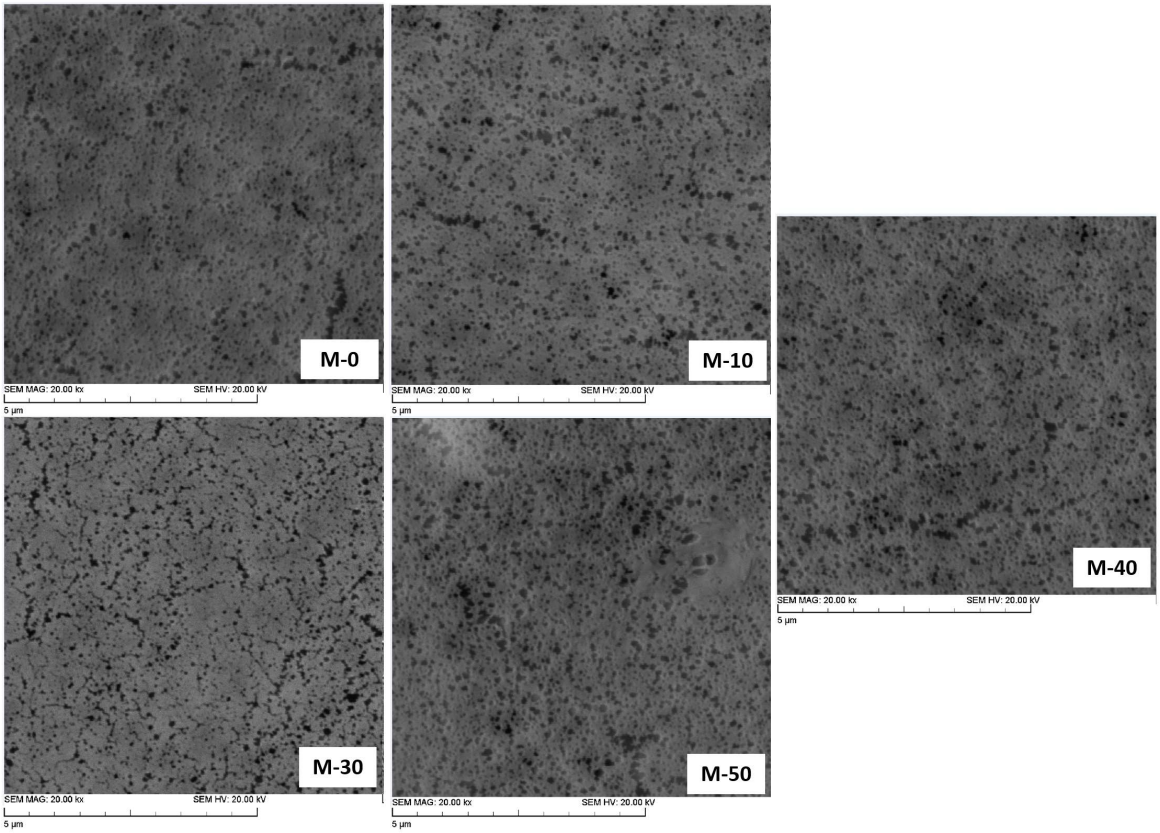

Fig. 4-2a SEM image of the prepared membranes at the top surface

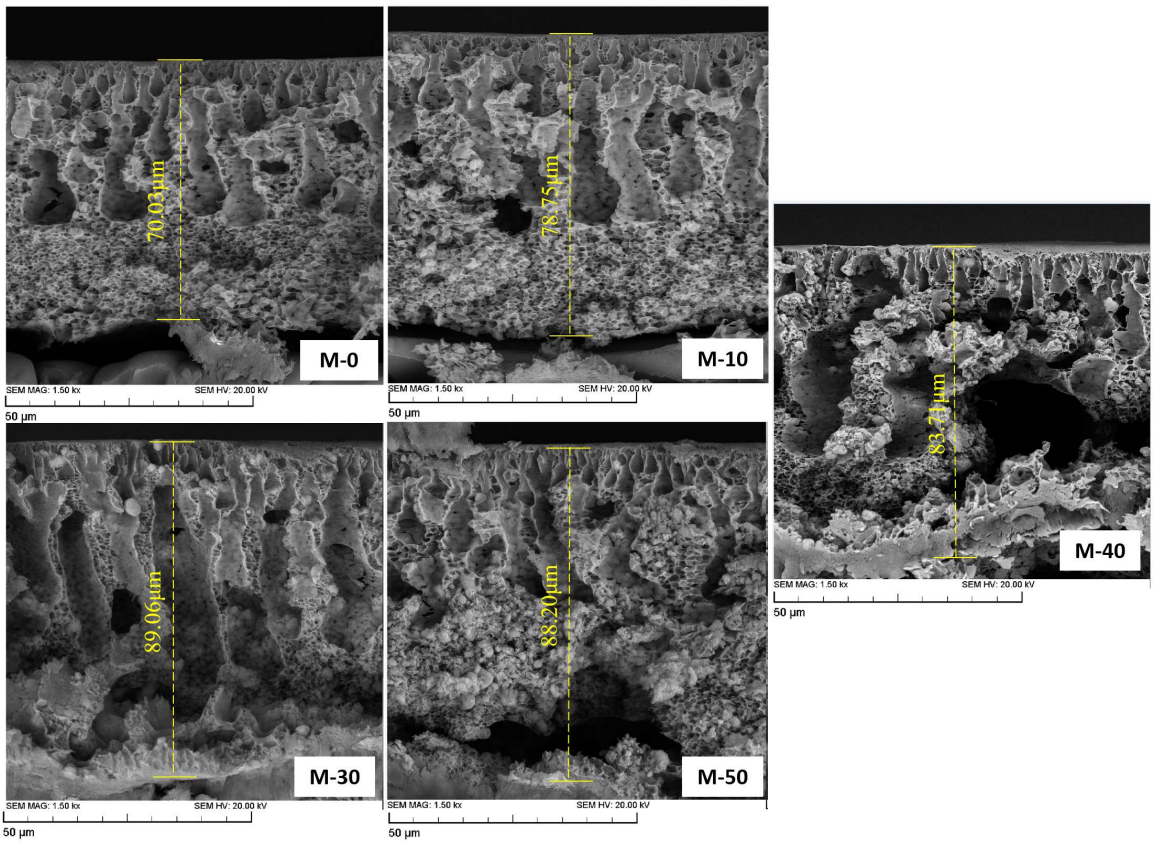

Fig. 4-2b Cross-sectional SEM images of the composite membranes

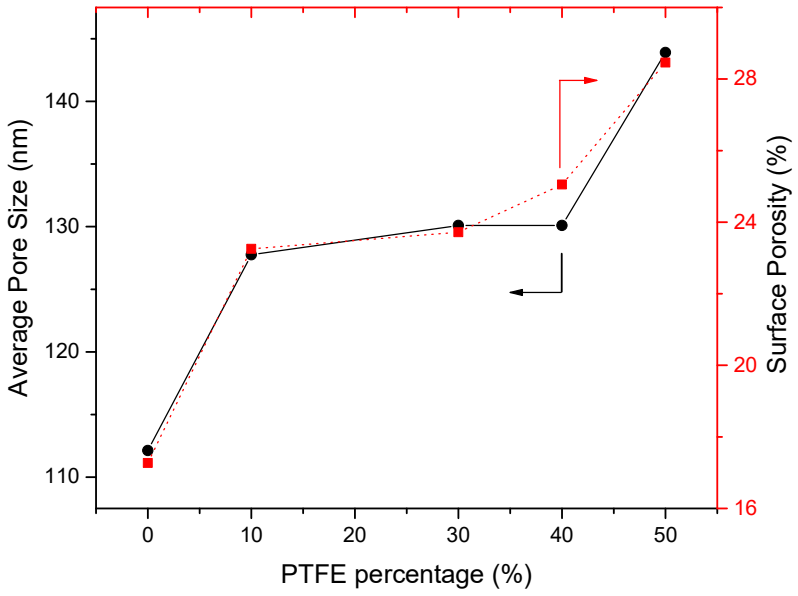

Fig. 4-3. Effect of PTFE concentration on surface porosity and average pore size

In term of the top surface morphology, as can be observed in Fig.4-2a and Fig.4-3, both average pore size and surface porosity of the PVDF-PTFE composite membranes are clearly higher than that of neat PVDF membrane and increase upon the increment of PTFE content in the composite membranes. From Fig.4-4, we can also see that the adding of PTFE material does not have a significant impact on the pore size distribution.

As for the cross-sectional morphology, the neat PVDF membrane shows a typical finger-like and sponge-like layer macro-void combined structure which was also mentioned in our previous works in Fig.4-2b.[14–16] However, as the PTFE contents in the composite membranes increases, the boundary between finger-like layer and sponge-like layer becomes undistinguished and the cross-sectional morphology presents a relatively continuous structure. The structure change could be attributed to the large particle size of the PTFE, which may disturb the polymer assembly during the membrane forming process. As also can be seen from Fig.4-2b, the thickness of the membrane top layer increase while the macro-void becomes larger with the increment of PTFE content initially which could tie with the increase of the total weight of polymer material and the scaffold effect that PTFE particles may play to the PVDF polymers in the membrane forming process. However, the top layer thickness achieves its highest limitation when the PTFE weight percent is 30% in the composite membranes. Then, the weight of polymers and particles may exceed the load-bearing ability of the PTFE particles in the composite membranes and the thickness of the membrane top layer stay nearly constant while more PTFE particles was further added

the macro-void inside the membranes was gradually fulfilled by the excess polymers and particles. Thus, when the content of PTFE reaches 50 wt%, the membranes shows a nearly solid structure in term of cross-sectional morphology.

4.3.2 ATR-FTIR

The analyzing results of ATR-FTIR were showed in Fig. 4-4, and only the data in the finger print zone (wavenumber 650 cm-1 to 1500 cm-1) was utilized to present a more clearly comparation between absorbance curves of different types of prepared membranes. And the absorbance curve of pure PVDF membrane was set as the base line to eliminate the impact of PVDF materials and only retain the impact of PTFE in the composite membranes, as the adsorption effect of PTFE is too weak to be detected for the PVDF-PTFE composite membranes. From Fig.4-4, all adsorption curves of the PVDF-PTFE composite membrane show the characteristic adsorption peak of PTFE material (wavenumber 1200 cm^{-1} and 1146 cm^{-1}) which demonstrates the inclusion of PTFE in the membranes and the membranes fabrication process did not cause any chemical change of the PTFE particles. And the adsorption peak of goes higher in the order of M-10, M-30, M-50, which reflects the fact that the PTFE content in the composite membranes increased.

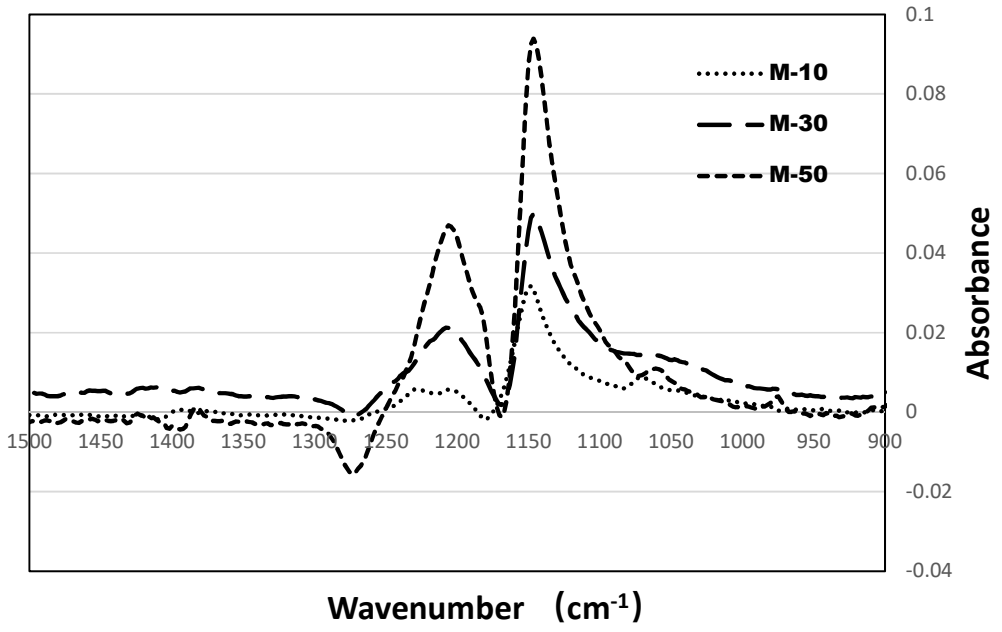

Fig. 4-4. ATR-FTIR images of the prepare membranes

4.3.3 Membrane porosity

As can be seen from the Figure 4-5, the porosity of prepared membranes drops slowly with the increment of PTFE content in the membranes initially and then drop sharply after extra PTFE was added. This could be explained by the SEM cross-sectional morphology images in Fig. 4-2b, which indicates the membranes become thicker and hollower on the visual with the adding of little amount of PTFE in the composite membranes. As also can be detected from Fig.4-2b, the extra PTFE particles and PVDF polymers would fill the membrane macro-voids when the total PTFE and PVDF polymer weight was further increased. However, the total weight of polymers increases with the adding of PTFE amount, which always demonstrate a decreasing porosity of the formed membranes.

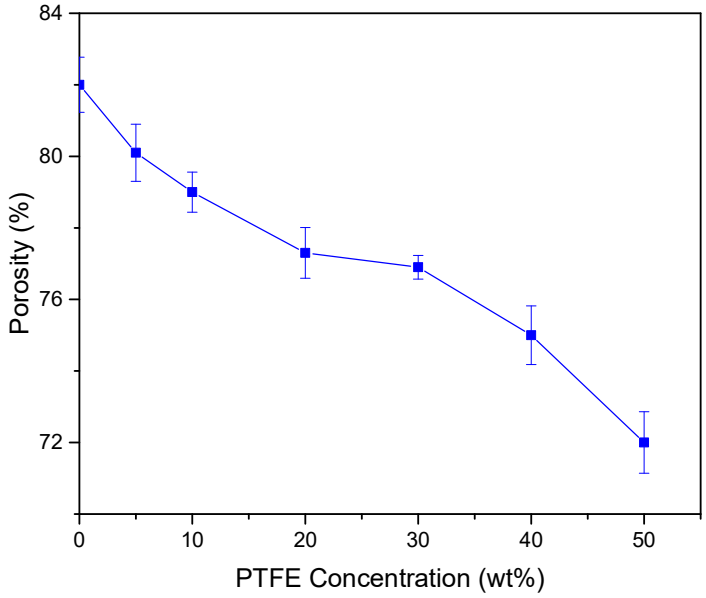

Fig. 4-5. Effect of PTFE concentration on membrane porosity

4.3.4 Water contact angle

The water contact angle data was presented in Fig.4-6 and the results illustrates a significant increasing trend in water contact angle with the increment of PTFE amount in the composite membranes. The results could be attributed to the relatively high hydrophobicity of PTFE materials which was added to the dope solution and partially distribute on the top surface of the formed membranes.

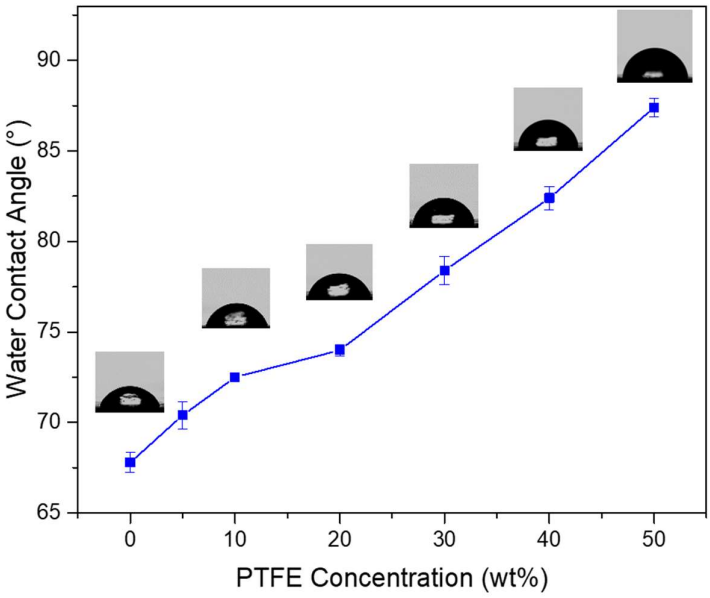

Fig. 4-6. Effect of PTFE concentration on membrane water contact angle

4.3.5 LEPw

Fig.4-7 presents the LEPw experimental results of the prepared membranes according to the PTFE concentrations. As can be observed from Fig.4-7, the LEPw value of the PTFE-PVDF composite membranes shows a significant decrease trend upon the adding of the PTFE particles. This could be explained by the increasing pore size and surface porosity, as shown in Fig.4-2, with the increment of the PTFE concentration in the composite membranes. However, the membrane thickness and porosity also increase upon the adding of the PTFE material, which well explains the deceleration of the LEPw decrement at high PTFE concentration in the membranes. It is worth mention that even the M-50 has the lowest LEPw value among these membranes, it is still

higher than 20 psi, which indicates a solid and durable enough membrane for VMD experiment and application.

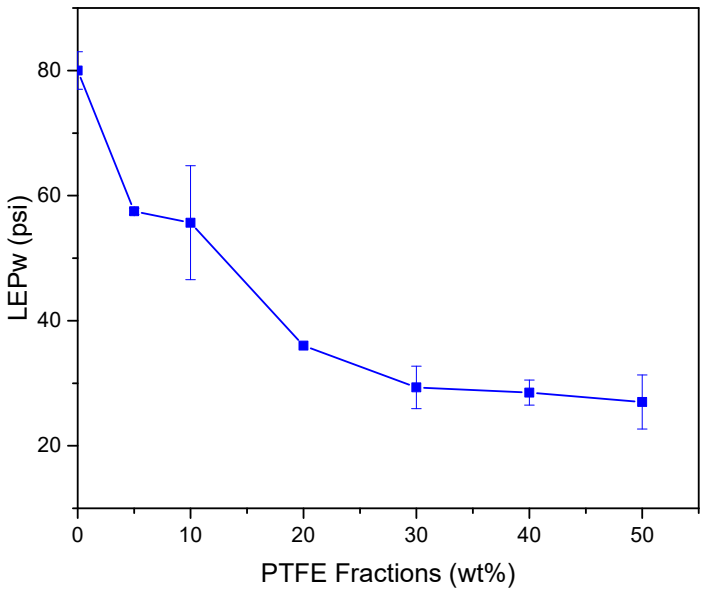

Fig. 4-7. Effect of PTFE concentration on membrane LEPw

4.3.6 VMD permeate flux and salt rejection

The pure water permeate flux data were shown in Fig.4-8 and the figure clearly shows a general increasing trend of permeate flux with the increment of PTFE content. This trend could be explained by the increasing pore size and surface porosity upon the increment of PTFE content, which can be observed in Fig.4-3. And the drop of permeate flux appears on M-50 could be attributed to the decreasing porosity which cause too much resistance to the vapor permeate through the membrane matrix. Considering the permeate flux and LEPw experimental results that were obtained for all prepared

membranes, we can tell M-40 is the most suitable membranes for VMD application which can be obtained in this study.

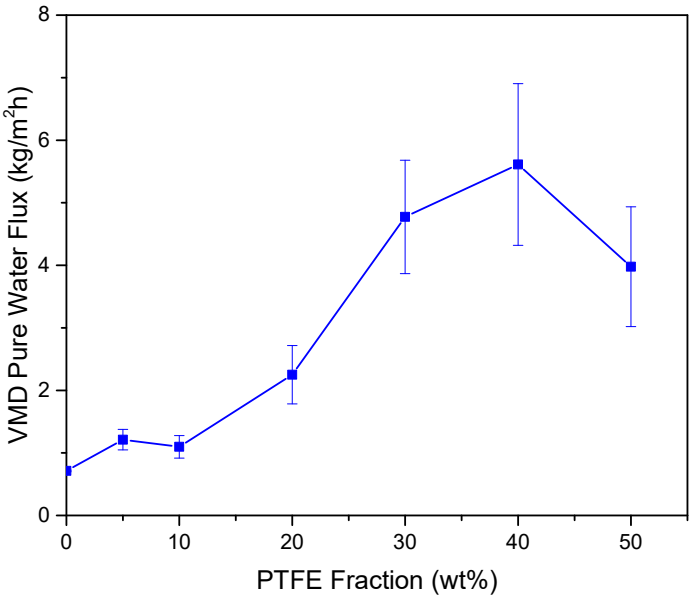

Fig. 4-8. Effect of PTFE concentration on membrane VMD pure water flux

Fig.4-9 presents the VMD experimental results using artificial seawater as feed. From Fig.4-9, the effect of concentration polarization could be observed clearly as the permeate flux values of all membranes are significantly lower than those when using pure water as feed. Different feed temperatures were also tested, and the permeate flux of all tested membranes increase with the increment of feed temperature. And the theoretical value of the VMD flux at different feed temperature were also shown in Fig.4-9, calculated using Antoine equation by setting the flux at 30℃ as base point.

$$p_{mf}(T_{mf}) = \exp(23.1964 - \frac{3816.44}{T_{mf} - 46.13}) \quad (4)$$

where p_{mf} and T_{mf} represent the partial vapor pressure and temperature at membrane surface on the feed side. And the pressure at membrane surface on the permeate side was assumed as vacuum during the calculation of trans-membrane pressure at different feed temperature. As shown in Fig. 4-9, the difference between the experimental and theoretical VMD permeate flux results for the tested membranes demonstrate a significant impact of temperature polarization and viscous flow of the transport vapor according to our previous works[14,18].

The salt rejection data was presented in Fig.4-10, and stable rejection performance for all tested membranes with the change of temperature were clearly demonstrated. It is also worth mention that, all rejection results are higher than 99.5%, which indicates excellent salt rejections of the prepared composite membranes.

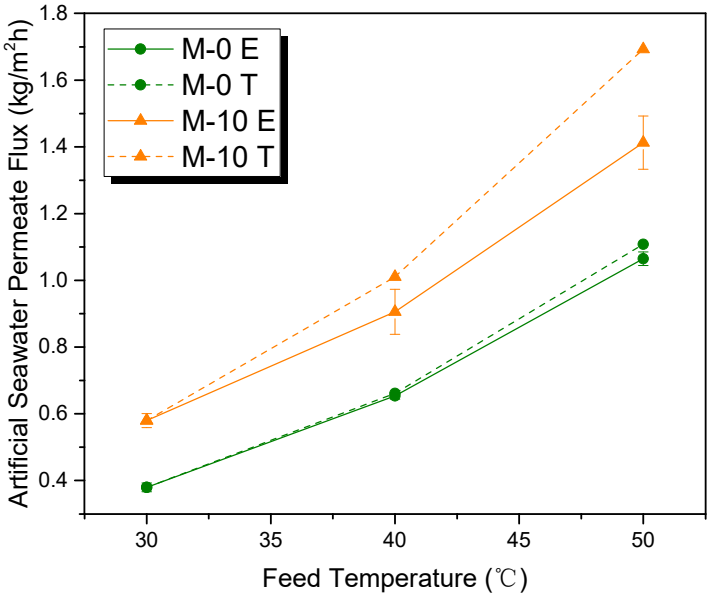

Fig. 4-9a. Effect of PTFE concentration on membrane VMD artificial seawater flux (low flux) (E: experimental result, T: theoretical result)

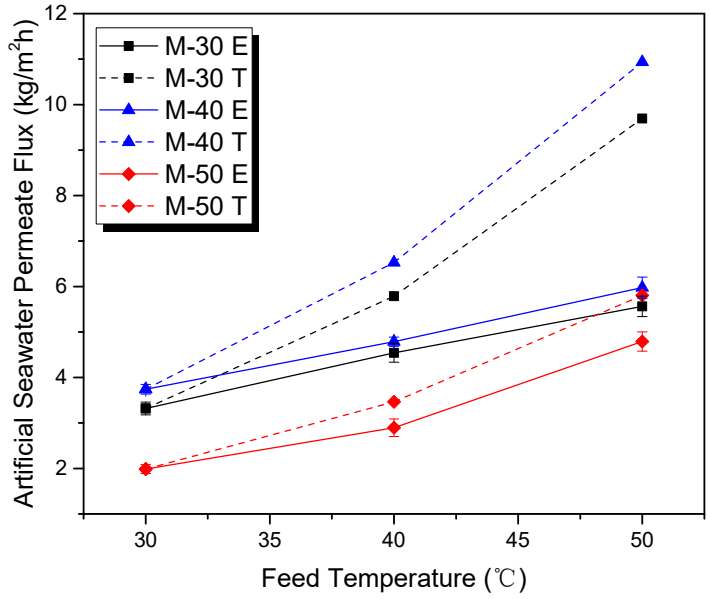

Fig. 4-9b. Effect of PTFE concentration on membrane VMD artificial seawater flux (high flux) (E: experimental result, T: theoretical result)

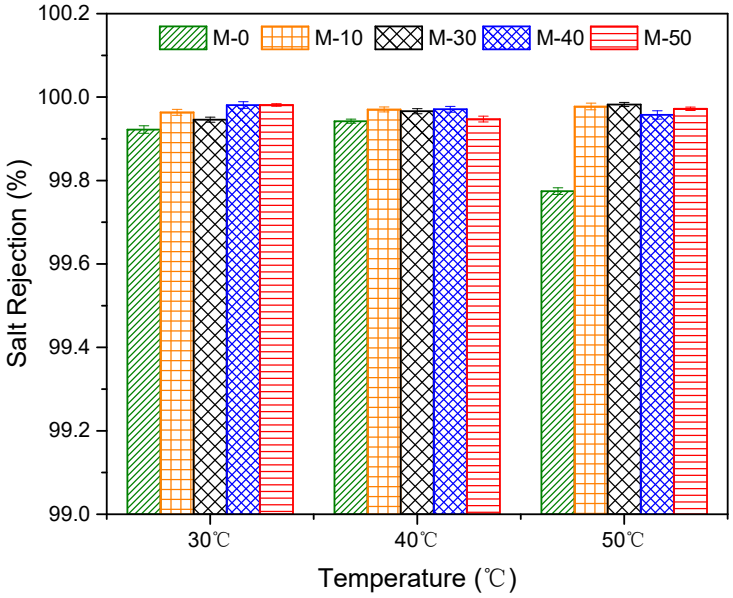

Fig. 4-10. Effect of PTFE concentration and feed temperature on membrane salt rejection

4.4 Conclusions

In this work, supported flat sheet PVDF-PTFE composite membranes were fabricated by the phase inversion process for the first time. Characterization such as, SEM, ATR-FTIR, contact angle measurement and LEPw test were carried out to test the prepared composite membranes. And the permeabilities of the membranes were detected by VMD experiments. The following conclusions can be drawn from this study:

1. Prepared PVDF-PTFE membranes have larger average pore size and higher surface porosity when compared with pure PVDF membranes. And both surface porosity and average pore size increase with the PTFE content in the composite membranes.

2. The adding of PTFE to the PVDF membrane changes the cross-sectional morphology of the membranes and the typical finger-like and sponge-like macro-void of pure PVDF membrane disappear gradually with the increment of the PTFE content in the membranes.

3. All PVDF-PTFE composite membranes prepared in this study exhibit better permeability in comparation with the pure PVDF membrane. And the VMD permeate flux of the M-40 could achieve 5.61 kg/m^{2}h, which is 690% higher than that of pure PVDF membrane.

4. Though PVDF-PTFE membranes have a larger average pore size and higher surface porosity, its LEPw performance is still higher than 20psi, which is sufficient for VMD applications.

5 The salt rejection performance of the prepared PVDF-PTFE composite membranes is sufficient and stable even when dealing with high temperature feeds, which indicates a applied type of distillation membrane for desalination applications.

Acknowledgements

The authors are thankful for the kind gift of the PVDF polymers by Arkema Inc. (Philadelphia, PA, U.S.A.). Financial supports from the NSERC Discovery and I2I

grants are also highly appreciated.

Reference

[1] N. Ghaffour, T.M. Missimer, G.L. Amy, Technical review and evaluation of the economics of water desalination: Current and future challenges for better water supply sustainability, Desalination. 309 (2013) 197–207. doi:10.1016/j.desal.2012.10.015.

[2] J. Yin, B. Deng, Polymer-matrix nanocomposite membranes for water treatment, J. Memb. Sci. 479 (2015) 256–275. doi:10.1016/j.memsci.2014.11.019.

[3] A.S. Hassan, H.E.S. Fath, Review and assessment of the newly developed MD for desalination processes, Desalin. Water Treat. 51 (2013) 574–585. doi:10.1080/19443994.2012.697273.

[4] T.H. Chong, S.L. Loo, A.G. Fane, W.B. Krantz, Energy-efficient reverse osmosis desalination: Effect of retentate recycle and pump and energy recovery device efficiencies, Desalination. 366 (2015) 15–31. doi:10.1016/j.desal.2015.01.017.

[5] R.K. McGovern, J.H. Lienhard V, On the potential of forward osmosis to energetically outperform reverse osmosis desalination, J. Memb. Sci. 469 (2014) 245–250. doi:10.1016/j.memsci.2014.05.061.

[6] L. Karimi, L. Abkar, M. Aghajani, A. Ghassemi, Technical feasibility comparison of off-grid PV-EDR and PV-RO desalination systems via their

energy consumption, Sep. Purif. Technol. 151 (2015) 82–94. doi:10.1016/j.seppur.2015.07.023.

[7] M.A.E.R. Abu-Zeid, Y. Zhang, H. Dong, L. Zhang, H.L. Chen, L. Hou, A comprehensive review of vacuum membrane distillation technique, Desalination. 356 (2015) 1–14. doi:10.1016/j.desal.2014.10.033.

[8] J.G. Lee, Y.D. Kim, W.S. Kim, L. Francis, G. Amy, N. Ghaffour, Performance modeling of direct contact membrane distillation (DCMD) seawater desalination process using a commercial composite membrane, J. Memb. Sci. 478 (2015) 85–95. doi:10.1016/j.memsci.2014.12.053.

[9] G. Guan, X. Yang, R. Wang, A.G. Fane, Evaluation of heat utilization in membrane distillation desalination system integrated with heat recovery, Desalination. 366 (2015) 80–93. doi:10.1016/j.desal.2015.01.013.

[10] W.G. Shim, K. He, S. Gray, I.S. Moon, Solar energy assisted direct contact membrane distillation (DCMD) process for seawater desalination, Sep. Purif. Technol. 143 (2015) 94–104. doi:10.1016/j.seppur.2015.01.028.

[11] Z.Q. Dong, X. hua Ma, Z.L. Xu, W.T. You, F. bing Li, Superhydrophobic PVDF-PTFE electrospun nanofibrous membranes for desalination by vacuum membrane distillation, Desalination. 347 (2014) 175–183. doi:10.1016/j.desal.2014.05.015.

[12] Q. lin Huang, C. fa Xiao, X. yu Hu, X. feng Li, Study on the effects and properties of hydrophobic poly(tetrafluoroethylene) membrane, Desalination. 277 (2011) 187–192. doi:10.1016/j.desal.2011.04.027.

[13] A. Razmjou, E. Arifin, G. Dong, J. Mansouri, V. Chen, Superhydrophobic modification of TiO 2 nanocomposite PVDF membranes for applications in membrane distillation, J. Memb. Sci. 415–416 (2012) 850–863. doi:10.1016/j.memsci.2012.06.004.

[14] Z. Li, D. Rana, Z. Wang, T. Matsuura, C.Q. Lan, Synergic effects of hydrophilic and hydrophobic nanoparticles on performance of nanocomposite distillation membranes: An experimental and numerical study, Sep. Purif. Technol. 202 (2018) 45–58. doi:10.1016/j.seppur.2018.03.032.

[15] J.E. Efome, M. Baghbanzadeh, D. Rana, T. Matsuura, C.Q. Lan, Effects of superhydrophobic SiO<inf>2</inf> nanoparticles on the performance of PVDF flat sheet membranes for vacuum membrane distillation, Desalination. 373 (2015) 47–57. doi:10.1016/j.desal.2015.07.002.

[16] M. Baghbanzadeh, D. Rana, C.Q. Lan, T. Matsuura, Effects of Inorganic Nano-Additives on Properties and Performance of Polymeric Membranes in Water Treatment, Sep. Purif. Rev. 45 (2016) 141–167. doi:10.1080/15422119.2015.1068806.

[17] Z. Chen, D. Rana, T. Matsuura, D. Meng, C.Q. Lan, Study on structure and vacuum membrane distillation performance of pvdf membranes: II. influence of molecular weight, Chem. Eng. J. 276 (2015) 174–184. doi:10.1016/j.cej.2015.04.030.

[18] Y. Yang, D. Rana, T. Matsuura, C.Q. Lan, The heat and mass transfer of vacuum membrane distillation: Effect of active layer morphology with and

without support material, Sep. Purif. Technol. 164 (2016) 56–62.

doi:10.1016/j.seppur.2016.03.023.

Chapter 5. Conclusions

Two types of PVDF-hosted composite distillation membranes, TiO_2 inorganic nanoparticles composite membrane and PVDF-PTFE composite membrane, were fabricated via phase inversion method in this study and applied to VMD process attempting to obtain a better permeability performance than pure PVDF membrane. And both type of membrane present much higher permeate flux than that of pure PVDF membrane, which illustrates the great potential of both these two fabrication strategies in distillation PVDF membrane performance enhancement. The best VMD permeate flux result of TiO_2 nanoparticle composite membrane and PVDF-PTFE composite membrane can achieve 4.26 kg/m^{2}h and 5.61 kg/m^{2}h, respectively, while that of pure PVDF membrane is only around 0.7 kg/m^{2}h. And it is also worth mention that, the LEPw and salt rejection ratio of the prepared membranes in this study were always in acceptable range, which further approve the applicability of the membranes fabricated by these two strategies in desalination and membrane distillation process.

In term of morphology change, both strategies could fabricate composite membranes with larger average pore size and higher surface porosity than pure PVDF membrane. However, pore size distribution didn't show significant change or shifting on membranes prepared based on any of these two strategies. For cross-sectional morphology, the addition of hydrophilic nanoparticle shows ability to increase the finger-like macro-void ratio while the addition of hydrophobic nanoparticles could grow the sponge-like macro-void. However, the finger-like and sponge-like layer

combined structure disappears gradually upon the introduction of PTFE materials in PVDF membrane attributed to the large particle size of PTFE which disturb the assembly of polymer during the membrane forming process. Besides, the membrane porosity decreases with the adding of both materials.

Finally, a synergistic effect of hydrophobic and hydrophilic TiO_2 nano-particles on membrane permeability and LEPw was found for the first time in the study of TiO_2 nanocomposite membrane fabrication.